DOI: 10.1002/chem.200600698

Luminescent Pt^{II}(bipyridyl)(diacetylide) Chromophores with Pendant Binding Sites as Energy Donors for Sensitised Near-Infrared Emission from Lanthanides: Structures and Photophysics of Pt^{II}/Ln^{III} Assemblies

Tanya K. Ronson,[a] Theodore Lazarides,[a] Harry Adams,[a] Simon J. A. Pope,[b] Daniel Sykes,[c] Stephen Faulkner,[c] Simon J. Coles,[d] Michael B. Hursthouse,[d] William Clegg,[e] Ross W. Harrington,[e] and Michael D. Ward*[a]

Abstract: The complexes [Pt(bipy){CC-(4-pyridyl)}$_2$] (**1**) and [Pt(*t*Bu$_2$bipy){CC-(4-pyridyl)}$_2$] (**2**) and [Pt(*t*Bu$_2$-bipy)-(CC-phen)$_2$] (**3**) all contain a Pt-(bipy)(diacetylide) core with pendant 4-pyridyl (**1** and **2**) or phenanthroline (**3**) units which can be coordinated to {Ln(diketonate)$_3$} fragments (Ln = a lanthanide) to make covalently-linked Pt^{II}/Ln^{III} polynuclear assemblies in which the Pt^{II} chromophore, absorbing in the visible region, can be used to sensitise near-infrared luminescence from the Ln^{III} centres. For **1** and **2** one-dimensional coordination polymers [**1**·Ln(tta)$_3$]$_\infty$ and [**2**·Ln(hfac)$_3$]$_\infty$ are formed, whereas **3** forms trinuclear adducts [**3**·{Ln(hfac)$_3$}$_2$] (tta = anion of thenoyl-trifluoroacetone; hfac = anion of hexafluoroacetylacetone). Complexes **1–3** show typical Pt^{II}-based ^{3}MLCT luminescence in solution at ≈510 nm, but in the coordination polymers [**1**·Ln(tta)$_3$]$_\infty$ and [**2**·Ln(hfac)$_3$]$_\infty$ the presence of stacked pairs of Pt^{II} units with short Pt···Pt distances means that the chromophores have ^{3}MMLCT character and emit at lower energy (≈630 nm). Photophysical studies in solution and in the solid state show that the ^{3}MMLCT luminescence in [**1**·Ln(tta)$_3$]$_\infty$ and [**2**·Ln(hfac)$_3$]$_\infty$ in the solid state, and the ^{3}MLCT emission of [**3**·{Ln(hfac)$_3$}$_2$] in solution and the solid state, is quenched by Pt→Ln energy transfer when the lanthanide has low-energy f–f excited states which can act as energy acceptors (Ln = Yb, Nd, Er, Pr). This results in sensitised near-infrared luminescence from the Ln^{III} units. The extent of quenching of the Pt^{II}-based emission, and the Pt→Ln energy-transfer rates, can vary over a wide range according to how effective each Ln^{III} ion is at acting as an energy acceptor, with Yb^{III} usually providing the least quenching (slowest Pt→Ln energy transfer) and either Nd^{III} or Er^{III} providing the most (fastest Pt→Ln energy transfer) according to which one has the best overlap of its f–f absorption manifold with the Pt^{II}-based luminescence.

Keywords: crystal structures · energy transfer · lanthanides · luminescence · platinum

Introduction

Near-infrared (NIR) luminescence from Ln^{III} complexes (Ln denotes a generic member of the lanthanide series) such as Pr^{III}, Nd^{III}, Er^{III} and Yb^{III} has become an area of intense interest because of its significant technological applications in areas ranging from medical imaging to optical communications.[1,2] Two particular problems associated with achieving

[a] T. K. Ronson, Dr. T. Lazarides, H. Adams, Prof. M. D. Ward
Department of Chemistry, University of Sheffield
Sheffield S3 7HF (UK)
Fax: (+44) 114-222-9484
E-mail: m.d.ward@sheffield.ac.uk

[b] Dr. S. J. A. Pope
School of Chemistry, Main Building, Cardiff University
Cardiff CF10 3AT (UK)

[c] D. Sykes, Prof. S. Faulkner
Department of Chemistry, University of Manchester
Oxford Road, Manchester M13 9PL (UK)

[d] Dr. S. J. Coles, Prof. M. B. Hursthouse
EPSRC National Crystallography Service, Department of Chemistry
University of Southampton, Highfield, Southampton SO17 1BJ (UK)

[e] Prof. W. Clegg, Dr. R. W. Harrington
School of Natural Sciences (Chemistry), University of Newcastle
Newcastle upon Tyne, NE1 7RU (UK)
and
CCLRC Daresbury Laboratory, Warrington WA4 4AD (UK)

Supporting information for this article is available on the WWW under http://www.chemeurj.org/ or from the author.

such NIR luminescence are i) the relatively low intensity and short lifetimes of the NIR-emitting lanthanides compared to visible-region emitters such as Eu^{III} and Tb^{III}, and ii) the low extinction coefficients of f–f absorptions, which means that sensitisation of the excited state by energy transfer from a strongly absorbing antenna group is usually necessary.[3] With regard to the first of these, two quite distinct strategies (use of highly encapsulating perfluorinated ligands, which allow neither solvent molecules nor C–H oscillators close to the metal;[4] and use of rate-limiting energy transfer from a d-block sensitiser[5]) have been notably successful in achieving remarkably long lifetimes for NIR emission from molecular Ln^{III} complexes.

With regard to the second problem—the requirement for highly absorbing sensitisers to act as antenna groups—a wide range of organic chromophores, either directly coordinated to the Ln^{III} centre or as pendant groups, have been employed.[6] In the last few years however attention has turned to the use of strongly-absorbing d-block chromophores as sensitisers for lanthanide-based luminescence.[5,7–9] This principle offers many advantages. The absorption maxima of d-block charge-transfer chromophores based on metals such as Re^{I}, Pt^{II}, Ir^{III}, Ru^{II}, Os^{II} span the entire visible region, such that more or less any excitation wavelength could be used by an appropriate choice of chromophore. Many of these complexes have relatively long-lived excited state (hundreds of nanoseconds or more) which makes energy transfer to a Ln^{III} centre competitive with radiative decay. Finally, the kinetic inertness of many of these d-block complexes means that they are very stable and can be used to assemble polynuclear d–f arrays using a "complexes as ligands" approach. Accordingly, we have used two approaches: i) the preparation of d-block complexes with vacant diimine binding sites to which a lanthanide(III) fragment can be bound in a separate step to give molecular d–f dinuclear complexes,[8] and ii) the preparation of coordination networks by combining cyanometallate chromophores such as $[Ru(bipy)(CN)_4]^{2-}$ with Ln^{III} cations, resulting in crystalline arrays containing Ru-CN-Ln bridges.[9] In both cases excitation of the d-block chromophore results in energy transfer to, and appearance of sensitised luminescence from, NIR-emitting Ln^{III} centres having low-energy f–f levels.

In this paper we describe the preparation of two new d-block chromophores based on the Pt(diimine)(diacetylide) core,[10] which have pendant N-donor groups (4-pyridyl, or 1,10-phenanthrolinyl) to which Ln^{III} complexes can bind. These Pt^{II} complexes show characteristically intense and long-lived emission,[10] and form polynuclear assemblies with lanthanides in which lanthanide-based sensitised emission occurs following d→f energy transfer. From the degree of quenching of the Pt-based luminescence, estimates of the rates of d→f energy transfer can be made for different Ln^{III} luminophores. The syntheses, structural, and photophysical properties of the new Pt^{II} complexes and their d–f assemblies are described.

Results and Discussion

Syntheses and structural properties of the new Pt complexes: The new Pt^{II} "complex ligands" are shown below. $[Pt(bipy)\{CC\text{-}(4\text{-}pyridyl)\}_2]$ (**1**) and $[Pt(t\mathrm{Bu}_2bipy)\{CC\text{-}(4\text{-}pyridyl)\}_2]$ (**2**) were prepared from the Cu^{I}-catalysed coupling of 4-ethynylpyridine with $[Pt(bipy)Cl_2]$ and $[Pt(t\mathrm{Bu}_2bipy)Cl_2]$, respectively; $[Pt(t\mathrm{Bu}_2\text{-}bipy)(CC\text{-}phen)_2]$ (**3**) was similarly prepared from $[Pt(t\mathrm{Bu}_2bipy)Cl_2]$ and 3-ethynyl-1,10-phenanthroline. The rationale behind the design of

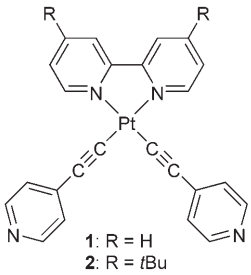

1: R = H
2: R = *t*Bu

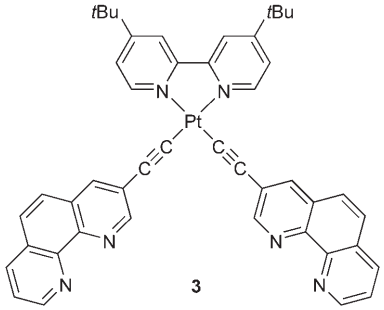

3

these was threefold. Firstly, the complexes have a pendant 4-pyridyl or 1,10-phenanthroline unit which is the site used for attachment to $Ln(diketonate)_3$ fragments to make the heteronuclear assemblies. Secondly, $Pt(diimine)(CCR)_2$ complexes are neutral and can be readily solubilised in low-polarity organic solvents, which will optimise the binding of the Ln^{III} fragments to the pendant N-donor sites; this association is strong in non-competitive solvents but does not occur in competitive solvents such as alcohols or MeCN. Thirdly, we[8d,11] and others[10c] have observed that attachment of electron-withdrawing substituents to the alkyne groups of $Pt(diimine)(CCR)_2$ complexes has a beneficial effect on luminescence, giving higher-energy and longer-lived luminescence compared to complexes where the R groups are not electron-withdrawing. These complexes are therefore expected be better energy donors than for example, $[Pt(bpym)(CCR)_2]$ (bpym = 2,2′-bipyrimidine) that we described earlier,[8d] where the vacant lanthanide-binding site is one side of the bipyrimidine ligand, resulting in a relatively low energy and short-lived Pt–bpym ^{3}MLCT excited state. We note that complex **2** was recently also described by Che and co-workers,[12] who were interested in the variations in solid-state luminescence of crystals when exposed to dif-

ferent organic solvent vapours; the use of this complex as a component of polynuclear assemblies has not previously been investigated.

We have structurally characterised both **1** and **2**; the structure we have obtained for **2**·0.5 CH_2Cl_2 is different from the alternative solvates **2**·CH_2Cl_2 and **2**·MeCN described by Che and co-workers.[12] The structures are shown in Figures 1 and 2, respectively. In **1** (Figure 1) the 4-pyridyl groups containing N(3) and N(4) are almost perpendicular to the mean plane of the bipy ligand, being twisted by 83.4 and 79.1°, respectively from the bipy mean plane; the molecules are arranged in alternating stacks with the 4-pyridyl groups directed to the outside of the stack and adjacent {Pt(bipy)} units (separated by a stacking distance of 3.3–3.4 Å) offset from one another such that there are no short Pt···Pt contacts. In **2**·0.5 CH_2Cl_2 the molecules are also arranged in stacks, but in pairs with two adjacent molecules having their 4-pyridyl groups pointing out of one side of the stack, and the next two molecules pointing in the other direction. Again the stacking involves the {Pt(bipy)} cores, with adjacent molecules offset such that there are no short Pt···Pt contacts. The pyridyl rings containing N(3) and N(4) are twisted from the plane of the 2,2′-bipyridyl fragment by 53.5 and 15.1°, respectively.

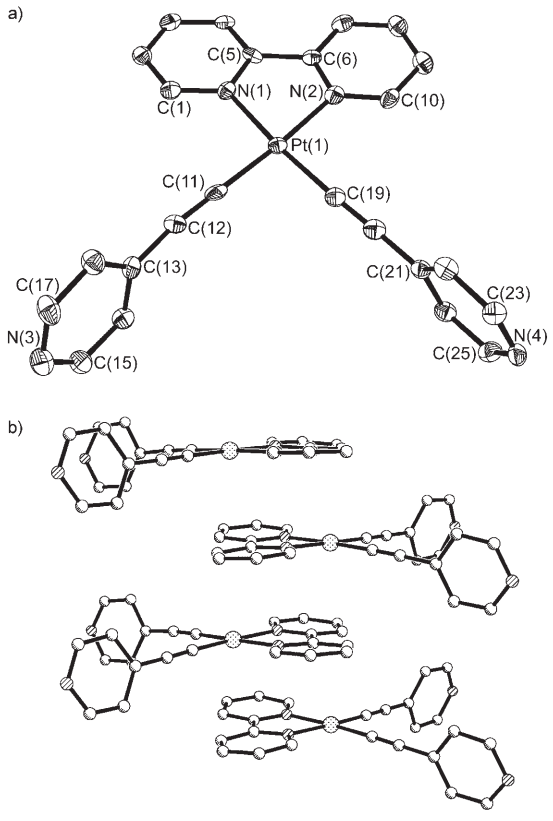

Figure 1. Two views of the structure of **1**: a) an ORTEP view showing 40% probability displacement ellipsoids, and the atom labelling scheme; b) the columnar stacking of molecules of **1**. H atoms are omitted for clarity. Selected bond lengths: Pt(1)–C(11) 1.939(8), Pt(1)–C(19) 1.956(8), Pt(1)–N(1) 2.054(6), Pt(1)–N(2) 2.062 Å.

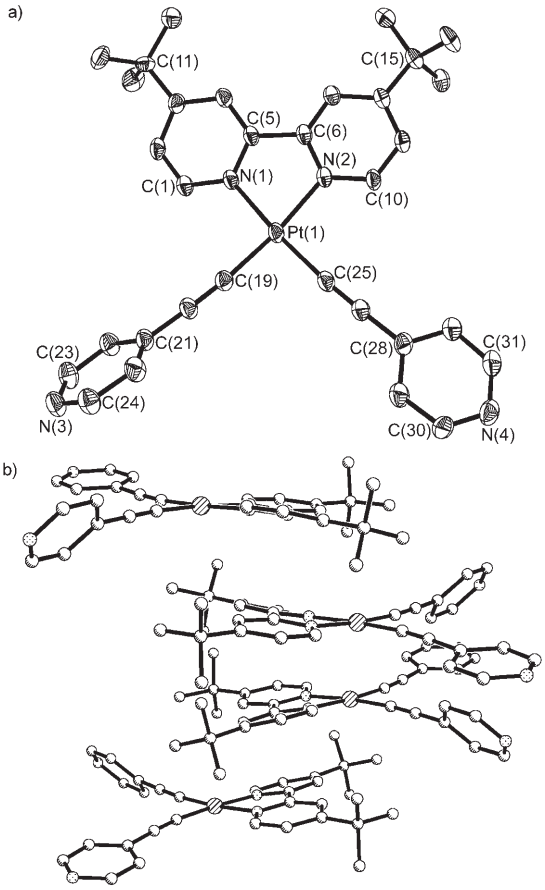

Figure 2. Two views of the structure of **2**·$(CH_2Cl_2)_{0.5}$: a) an ORTEP view showing 40% probability displacement ellipsoids, and the atom labelling scheme; b) the columnar stacking of molecules of **2**. H atoms are omitted for clarity. Selected bond lengths: Pt(1)–C(19) 1.942(5), Pt(1)–C(26) 1.946(5), Pt(1)–N(1) 2.054, Pt(1)–N(2) 2.057 Å.

Syntheses and structures of Pt^{II}–Ln^{III} polynuclear complexes: Ln^{III} tris(diketonate)dihydrates [Ln(diketonate)$_3$-$(H_2O)_2$] form adducts with one bidentate or two monodentate N-donor ligands such as pyridines in non-polar solvents; this is the principle we have exploited before for assembly of heterodinuclear d–f complexes.[8] Accordingly, we combined complexes **1** or **2** with [Ln(hfac)$_3$$(H_2O)_2$] or [Ln(tta)$_3$-$(H_2O)_2$] (Hhfac = hexafluoroacetylacetone; Htta = thenoyltrifluoroacetone; Ln = Gd, Pr, Nd, Er, Yb) in CH_2Cl_2 to afford reasonable yields of orange crystalline products for which elemental analysis was consistent with a 1:1 association of Pt^{II} complex (**1** or **2**) and {Ln(diketonate)$_3$} unit.

The structures of these adducts proved to be interesting. Duan, Yanagida and co-workers recently prepared adducts of $[Ru(bipy)_2(4,4'\text{-bipy})_2]^{2+}$ (which, like **1** and **2**, contains two externally-directed 4-pyridyl groups at approximately 90° to one another) with {Ln(tta)} fragments which were proposed on the basis of mass spectroscopic data to be Ru_2Ln_2 molecular squares.[7g] Our adducts however are, in the solid state, all one-dimensional coordination polymers with alternating Pt^{II} and Ln^{III} centres. Members of two

series have been structurally characterised: as representative examples the structure of $[\mathbf{1}\cdot Yb(tta)_3]_\infty$ is in Figures 3 and 4, and that of $[\mathbf{2}\cdot Er(hfac)_3]_\infty$ is in Figures 5 and 6.

The structure of $[\mathbf{1}\cdot Yb(tta)_3]_\infty$ (Figure 3, Figure 4) is a zig-zag chain with the 90° kinks occurring at the Pt^{II} centres because of the *cis* arrangement of the two pendant 4-pyridyl units. Each Yb^{III} centre is eight-coordinate from the three bidentate tta ligands and two monodentate pyridyl ligands, each from a different Pt^{II} unit. The N-Yb-N angle is 144.6°; the coordination geometry around Yb^{III} is a typical square-antiprism with N(3), O(3), O(4) and O(5) constituting one approximate square plane, and N(4), O(1), O(2) and O(6) the other one. The Pt···Yb distances within the chain are very similar at 9.92 and 9.88 Å.

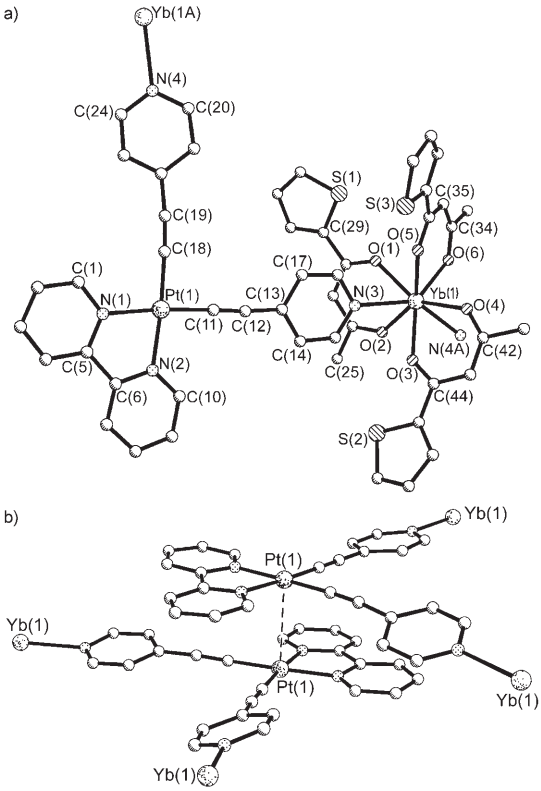

Figure 3. Parts of the structure of $[\mathbf{1}\cdot Yb(tta)_3\cdot(CH_2Cl_2)_{1.5}]_\infty$. a) The contents of the asymmetric unit, showing the atom labelling scheme; Yb(1A) and N(4A) from neighbouring asymmetric units have been added to illustrate the complete coordination spheres around the metal ions. H and F atoms and solvent molecules are omitted for clarity. b) A view of two units of the Pt^{II} fragment **1** from adjacent chains, showing the Pt···Pt contacts. Yb–O separations vary from 2.249(3) Å [Yb(1)–O(6)] to 2.320(3) [Yb(1)–O(1)], Yb(1)–N(3) 2.526 Å, Yb(1)–N(4A) 2.495 Å. For details of the isostructural Er^{III} analogue, see Supporting Information.

An interesting feature of the complex is that {Pt(bipy)} units from adjacent chains are stacked together in pairs such that there is a Pt···Pt separation of 3.334 Å approximately perpendicular to the zig-zag chain; this is shown in Figure 3b. Note that this is not accompanied by aromatic π–π stacking between the bipyridyl ligands which are spatially

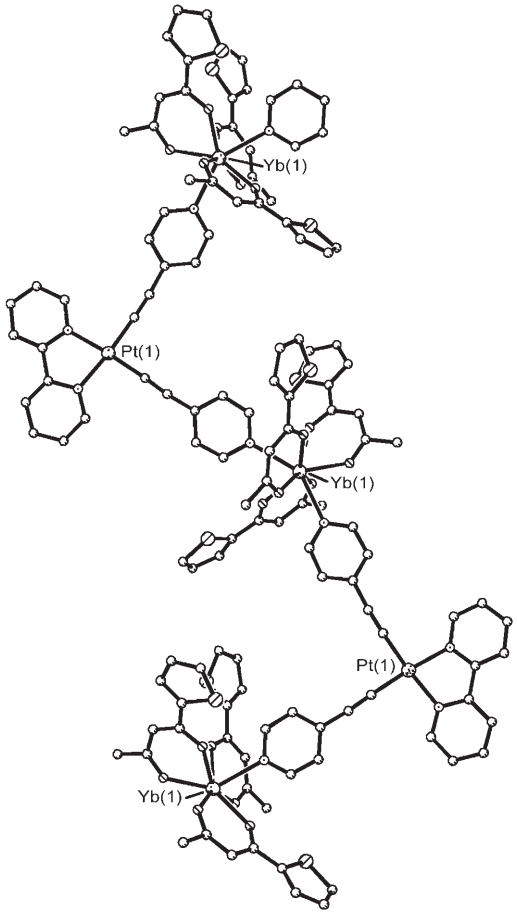

Figure 4. Chain structure of $[\mathbf{1}\cdot Yb(tta)_3\cdot(CH_2Cl_2)_{1.5}]_\infty$.

separated and lie on opposite sides of the Pt···Pt bond. Each $(Pt\text{-}Yb\text{-})_\infty$ chain is associated in this way with two others, one on each side of it, via Pt···Pt interactions in which all Pt^{II} centres are involved. An important consequence of this from the point of view of the photophysical properties is that the light-harvesting chromophore which will transfer its excitation energy to the Ln^{III} luminophores is no longer a Pt^{II} monomer but a $\{Pt^{II}\}_2$ unit. The presence of Pt···Pt interactions is well known to change the photophysical characteristics of Pt^{II}–diimine complexes, with the lowest-energy excited state changing from (usually) ^{3}MLCT excited state in monomers to ^{3}MMLCT (metal–metal bond to ligand charge-transfer) in stacked dimers or oligomers in which there is a metal-metal bonding interaction.[13] The complex $[\mathbf{1}\cdot Er(tta)_3]_\infty$ is isostructural and isomorphous, with a Pt···Pt distance of 3.337 Å in the associated Pt^{II} pairs.

$[\mathbf{2}\cdot Er(hfac)_3]_\infty$ has a basically similar alternating chain structure (Figures 5, 6), although there are two crystallographically independent formula units such that the chain has a $\{Pt(1)\text{-}Er(1)\text{-}Pt(2)\text{-}Er(2)\text{-}\}_\infty$ sequence and is not just a simple alternating "zig-zag". Again the Er^{III} centres are eight-coordinate with an approximately square antiprismatic coordination environment: for Er(1) the two approximate square planes consist of donor atoms N(3)/O(3)/O(4)/O(6)

and N(7)/O(1)/O(2)/O(5); for Er(2) the two approximate square planes consist of N(4)/O(9)/O(11)/O(12) and N(8)/O(7)/O(8)/O(10). Along the Pt(1)-Er(1)-Pt(2)-Er(2)-Pt(1) sequence of complex fragments the Pt···Er separations are 9.83, 9.87, 9.85 and 9.92 Å, respectively.

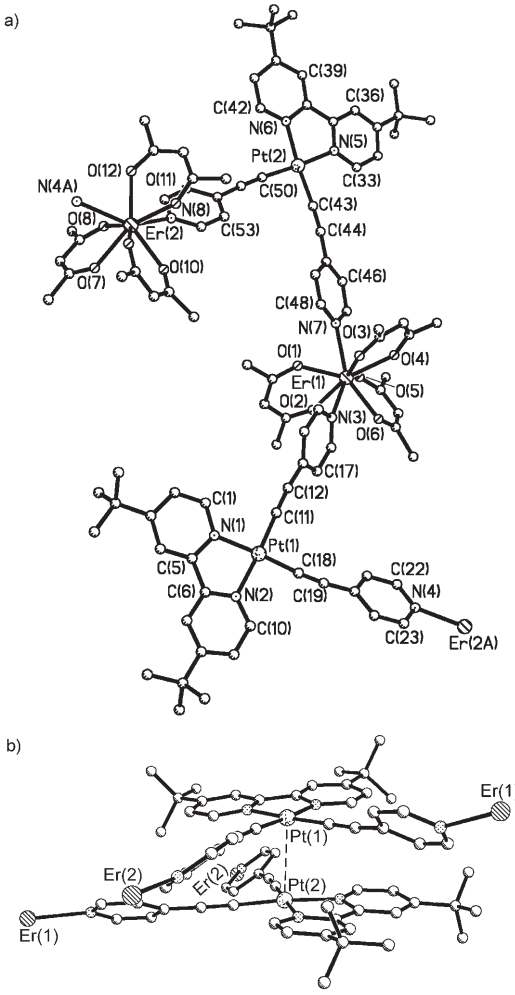

Figure 5. Parts of the structure of $[\mathbf{2}{\cdot}Er(hfac)_3{\cdot}(CH_2Cl_2)]_\infty$. a) The contents of the asymmetric unit, showing the atom labelling scheme; Er(2A) and N(4A) from neighbouring asymmetric units have been added to illustrate the complete coordination spheres around the metal ions. H and F atoms and solvent molecules are omitted for clarity. b) A view of two units of the Pt^{II} fragment **2** from adjacent chains, showing the Pt···Pt contacts. Er–O separations range from 2.281(6) Å [Er(1)–O(3)] to 2.332(6) Å [Er(1)–O(5)], Er(1)–N(7) 2.515(8), Er(1)–N(3) 2.540(7), Er(2)–N(4A) 2.531(8), Er(2)–N(8) 2.556 Å. For details of the isostructural Yb^{III} analogue see Supporting Information.

Again, a Pt···Pt interaction between adjacent chains is present, with the Pt···Pt separation being 3.248 Å. These pairs are between crystallographically inequivalent Pt centres, that is, every Pt(1) interacts with a Pt(2) such that all Pt···Pt interactions are equivalent; see Figure 5b. As before, there is no π–π aromatic stacking between the associated bipyridyl ligands and any perturbation that this association causes to the photophysical properties will arise from the

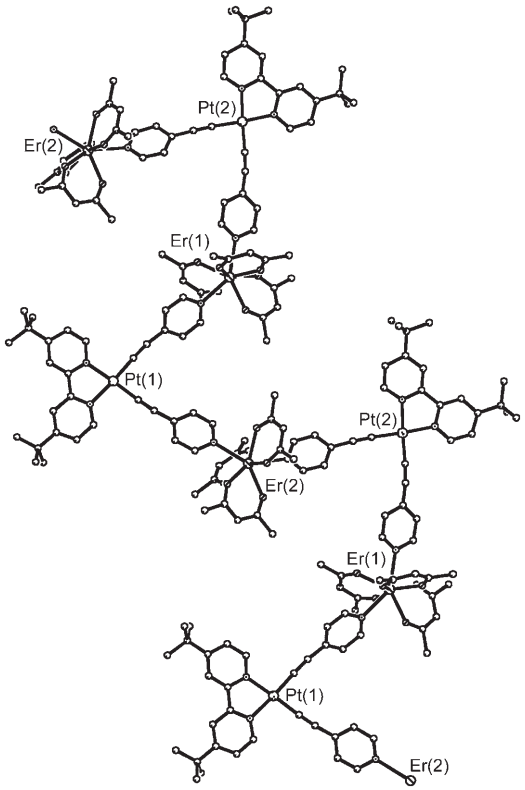

Figure 6. Chain structure of $[\mathbf{2}{\cdot}Er(hfac)_3{\cdot}(CH_2Cl_2)]_\infty$.

Pt···Pt interaction only. The complex $[\mathbf{2}{\cdot}Yb(hfac)_3]$ is isostructural and isomorphous, with a separation of 3.252 Å between the Pt atoms in the Pt(1)···Pt(2) pairs.

Complex **3**, in contrast to **1** and **2**, is not expected to form coordination networks, but can form trinuclear $PtLn_2$ complexes by attachment of a $\{Ln(diketonate)_3\}$ fragment at each of the two pendant phenanthroline sites. Such complexes were simply prepared by reaction of **3** with two equivalents of $[Ln(hfac)_3(H_2O)_2]$ in CH_2Cl_2/heptane; the structure of $[\mathbf{3}{\cdot}\{Yb(hfac)_3\}_2]$ is shown in Figure 7. The geometric parameters associated with the planar Pt^{II} and eight-coordinate square-antiprismatic Yb^{III} centres are unremarkable. For Yb(1) the two square planes in the coordination environment consist of O(7)/O(8)/O(9)/O(10) and N(5)/N(6)/O(11)/O(12); for Yb(2) the two square planes consist of O(3)/O(4)/O(5)/O(6) and N(3)/N(4)/O(1)/O(2). The two Yb^{III} units are close together [Yb(1)···Yb(2) separation, 10.83 Å] with contacts of 2.7–2.9 Å between F atoms associated with the separate $\{Yb(hfac)_3\}$ units. The Pt···Yb separations are 8.39 Å to Yb(1) and 8.28 Å to Yb(2).

Photophysical properties of the Pt^{II} complexes and their Ln^{III} adducts

i) Properties of the mononuclear Pt^{II} complexes 1–3: Complexes **1** and **2** are yellow due to absorption maxima at 389 and 381 nm, respectively which we ascribe to an MLCT transition, as for other Pt^{II}–diimine–di(acetylide) complex-

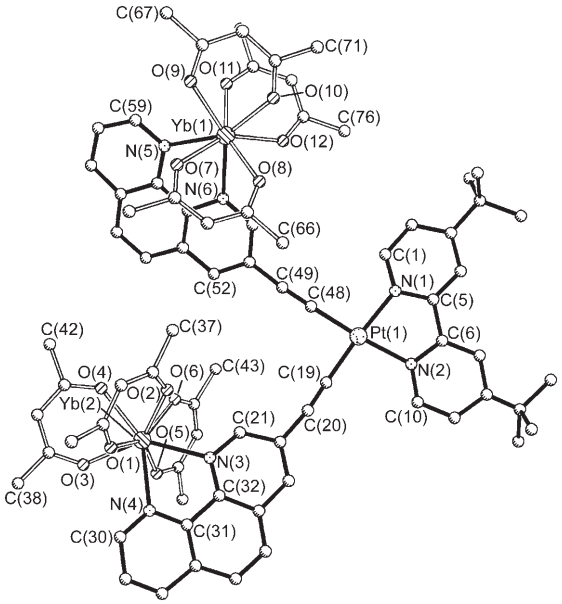

Figure 7. Structure of $[\mathbf{3}\cdot\{Yb(hfac)_3\}_2\cdot(CH_2Cl_2)_{1.5}]$ showing the atom labelling scheme. H and F atoms and solvent molecules are omitted for clarity. The bonds associated with the hfac ligands are shown hollow. Selected bond lengths: Pt(1)–N(1) 2.064(8), Pt(1)–N(2) 2.060(8), Pt(1)–C(19) 1.966(9), Pt(1)–C(48) 1.950(10), Yb(1)–N(5) 2.467(9), Yb(1)–N(6) 2.458(8), Yb(2)–N(3) 2.441(8), Yb(2)–N(4) 2.485(9) Å. Yb-O separations are in the range 2.276(8) Å [Yb(1)–O(10)] to 2.323(7) Å [Yb(2)–O(2)].

es.[10b] They are strongly luminescent in aerated fluid solution with emission maxima at 508 and 520 nm, respectively, with quantum yields of $> 5\%$ and lifetimes of 139 and 105 ns. This behaviour is typical for complexes of this type.[10] At high concentrations (> 1 mM) the more soluble complex **2** shows an additional weak emission maximum at 700 nm (Figure S1) which becomes more apparent as the concentration increases. This is again typical behaviour of planar Pt^{II} complexes of this type[13] and arises from association in solution in one of two ways: π–π stacking between aromatic ligands to generate excimer emission, or a Pt···Pt interaction to generate emission from a ^{3}MMLCT excited state in which the excited electrons come not from a single Pt^{II} centre but a $\{Pt^{II}\}_2$ pair with a weak metal–metal bond.[13g,h] In both cases the excited state is lower in energy than in the corresponding monomeric complex. It is not apparent which type of interaction is occurring in the solution of **2** at these concentrations, however, we note that whereas both **1** and **2** show intramolecular π–π stacking in their crystal structures, neither structure displays Pt···Pt interactions, and on this basis we assign the 700 nm emission feature at high concentrations of **2** to a π-stacked excimer. Complex **1** was not sufficiently soluble in CH_2Cl_2 to allow these high concentrations to be achieved.

In the solid state, as microcrystalline powders, **1** and **2** display more structured luminescence (Figure 8) but with the main maximum in the same region (e.g. 514 nm for **1**). The presence of additional lower-energy features at about 550 and 600 nm that are not present in the solution luminescence spectra suggests a vibrational progression than is not apparent in solution;[13e] in addition there may be a contribution from some excimer emission arising from the stacked bipyridyl ligands in the solid state.[13d–f] We can be sure however that these low energy features do *not* arise from MMLCT processes in the solid state because there are no short Pt···Pt contacts in either crystal structure. UV/Vis and luminescence data are collected in Table 1.

Table 1. Summary of absorption and luminescence data.

Complex	λ_{max} [nm] [$10^{-3}\varepsilon$ in $M^{-1}cm^{-1}$]	λ_{em} [nm]	τ [ns]
1[a]	389 (8.2), 287 (49)	508	139
2[a]	381 (9.6), 288 (53)	520	105
3[a]	375 (≈30; sh), 333 (80), 320 (84), 279 (114)	526	324

Complex	τ(Pt) [ns][c] fitting method **A**	fitting method **B**	τ(Ln) [μs][d]
1·Gd(tta)$_3$[b]	692(80%), 346(20%)	578	–
1·Yb(tta)$_3$[b]	273(98%), 66(2%)	259	9.76
1·Er(tta)$_3$[b]	27(80%), 45(20%)	29	1.67
1·Pr(tta)$_3$[b]	20(67%), 49(33%)	25	0.86
1·Nd(tta)$_3$[b]	≈10 (very weak)	≈10	1.02
2·Gd(hfac)$_3$[b]	819(92%), 371(7%)	768	-
2·Yb(hfac)$_3$[b]	476(90%), 217(10%)	413	8.24
2·Er(hfac)$_3$[b]	52(80%), 124(20%)	56	1.58
2·Nd(hfac)$_3$[b]	≈10 (very weak)	≈10	0.71, 0.54
3·$\{Gd(hfac)_3\}_2$[a,e]	835		–
3·$\{Yb(hfac)_3\}_2$[a,e]	17		11.1 (11.6)[f]
3·$\{Er(hfac)_3\}_2$[a,e]	≈1 (very weak)		1.64
3·$\{Nd(hfac)_3\}_2$[a,e]	7		1.08 (1.00)[f]

[a] Measured in air-equilibrated CH_2Cl_2 solution; the Pt-based emission at ≈520 nm arises from a ^{3}MLCT excited state (see main text). [b] Measured on a solid-state powder sample; the Pt-based emission at ≈630 nm arises from a ^{3}MMLCT excited state (see main text). [c] Luminescence from the Pt^{II} chromophore in the visible region. For series **1** and **2** (measured in the solid state), the lifetimes obtained allowing a two-component exponential fit, with their relative weightings as percentages, are in the first column (method **A**). The corresponding "weighted average" lifetimes obtained by only allowing a single-component exponential fit to the time-resolved emission profile are in the second column (method **B**); these fit the data less well than the two-component fits but have been taken as an average value for calculation of energy-transfer rates (see main text). For series **3** the emission lifetimes were only measured in solution so this issue does not arise and all emission profiles gave clean single-exponential fits. [d] Sensitised luminescence from the Ln^{III} centre in the near-IR region, measured at the wavelength of the most intense emission feature for each Ln^{III} ion [Yb, 980 nm ($^2F_{5/2}\rightarrow{}^2F_{7/2}$); Er, 1530 nm ($^4I_{13/2}\rightarrow{}^4I_{15/2}$); Nd, 1065 nm ($^4F_{3/2}\rightarrow{}^4I_{11/2}$); Pr, 1050 nm ($^1D_2\rightarrow{}^3F_4$): see Figure S2, Supporting Information for representative emission spectra]. Excitation was into the Pt^{II}-based MLCT absorption band in every case ($\lambda_{exc}=440$ or 532 nm) so that no significant direct excitation of the Ln^{III} unit occurred. [e] Prepared in situ in solution by addition of 2 equiv of the appropriate $[Ln(hfac)_3\cdot 2H_2O]$ to one equivalent of **3** in solution. [f] Value in parentheses determined from a powder sample to compare with the solution value (immediately preceding).

Complex **3** shows in its UV/Vis spectrum in dilute solution a broad area of absorbance between about 360 and 420 nm, with a just-discernable maximum at 390 nm, in the region expected for MLCT absorptions. The corresponding luminescence in aerated CH_2Cl_2 solution occurs at 526 nm with a lifetime of 324 ns.

ii) Photophysical properties of the coordination polymers $[\mathbf{1}\cdot Ln(tta)_3]_\infty$ and $[\mathbf{2}\cdot Ln(hfac)_3]_\infty$ in the solid state: The coordination polymers $[\mathbf{1}\cdot Ln(tta)_3]_\infty$ and $[\mathbf{2}\cdot Ln(hfac)_3]_\infty$ (Ln = Gd, Pr, Nd, Er, Yb) show quite different solid-state luminescence behaviour from the mononuclear Pt^{II} complexes **1** and **2**, because of i) the presence of stacked Pt_2 dinuclear units in the crystal, and ii) the presence of the lanthanide complex unit which (in all cases except Ln = Gd) has low-energy f–f excited states which can quench the excited state of the Pt–bipy chromophores and become sensitised itself to give near-IR luminescence.[5,7–9] The solid-state luminescence in the visible region of the series $[\mathbf{1}\cdot Ln(tta)_3]_\infty$, following excitation into the Pt-based absorption manifold at either 440 or 532 nm, is shown in Figure 8. We consider first the behaviour of $[\mathbf{1}\cdot Gd(tta)_3]_\infty$ (dotted line in the figure) as in this case there can be no quenching of Pt-centred luminescence by Gd^{III} whose lowest energy excited state lies at about 32000 cm^{-1}, in the UV region. This complex shows broad, unstructured emission at 635 nm which must arise from the Pt^{II} centres. It is considerably red-shifted compared to the luminescence maxima for monomeric **1** in solution (508 nm) and also in the solid state (514 nm); given the short Pt···Pt contacts in the solid state involving all Pt^{II} centres, this luminescence can confidently be ascribed to ^{3}MMLCT luminescence from the pairs of interacting Pt^{II} units in the crystals.[13] It is at a significantly shorter wavelength from the excimer emission at 700 nm that was observed in solutions of **2** at high concentrations (see above), consistent with it having a different origin. The fact that there is no evidence for any monomer emission at ≈510 nm from $[\mathbf{1}\cdot Gd(tta)_3]_\infty$ also supports this assignment. As with other solid-state coordination networks that we have investigated,[9] the time-resolved luminescence decay did not correspond to a clean single-exponential process, but fitted much better to two components with lifetimes of 692 and 346 ns, with the former being the dominant component (about 4:1). This cannot be ascribed to crystallographically inequivalent Pt^{II} environments, but likely arises because of in homogeneities in the solid-state sample (e.g. crystal defects; difference between surface and bulk environments in a finely-ground sample). For the purposes of estimating energy-transfer rates we have also generated a weighted-average lifetime (578 ns) which is the best fit to the time-resolved emission profile that could be obtained from a single-exponential function; these "average" lifetime values are also included in Table 1. This value of 578 ns is considerably longer than the lifetime for monomeric **1**, which will in part due to the different nature of the emitting excited state (^{3}MMLCT for $[\mathbf{1}\cdot Gd(tta)_3]_\infty$ instead of ^{3}MLCT for **1**), but the additional electron-withdrawing effect arising from coordination of Gd^{III} units to the pendant pyridyl groups of **1** may also be significant.[8d,10c,11]

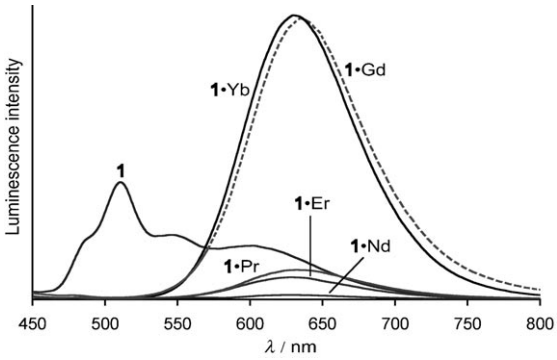

Figure 8. Solid-state luminescence spectra (powdered samples) of complex **1**, and the series $[\mathbf{1}\cdot Yb(tta)_3\cdot(CH_2Cl_2)_{1.5}]_\infty$.

As the Ln^{III} ion is changed through the rest of the series $[\mathbf{1}\cdot Ln(tta)_3]_\infty$ the Pt-based emission intensity diminishes in the order Yb > (Pr ≈ Er) > Nd, which is very similar to behaviour that we have seen before in coordination networks based on cyanide-bridged $[Ru(bipy)(CN)_4]^{2-}/Ln^{3+}$ networks.[9b] Whilst the absolute intensities of solid-state luminescence spectra cannot be compared as reliably as solution spectra, it is clear that the Pt-based luminescence remains strong in $[\mathbf{1}\cdot Yb(tta)_3]_\infty$; it is considerably weaker for $[\mathbf{1}\cdot Er(tta)_3]_\infty$ and $[\mathbf{1}\cdot Pr(tta)_3]_\infty$; and it is almost completely quenched for $[\mathbf{1}\cdot Nd(tta)_3]_\infty$ (Figure 8). This trend is borne out by time-resolved measurements on the solids across the series $[\mathbf{1}\cdot Ln(tta)_3]_\infty$, for which the weighted-average lifetimes of the Pt-based luminescence decay at 630 nm are 259 ns (Ln = Yb), 29 ns (Ln = Er), 25 ns (Ln = Pr) and < 10 ns (almost undetectable, for Ln = Nd). We emphasise again that the heterogeneity of crystalline samples and possible surface effects result in luminescence decay profiles that are not clean single-exponentials like those observed in solution, so these lifetimes are subject to larger uncertainty than usual. The general trend however, on the basis of both steady-state luminescence intensities and time-resolved measurements, is perfectly clear: Yb^{III} is a relatively poor quencher of Pt^{II}-centred ^{3}MMLCT emission in this series, Nd^{III} is the most effective quencher, and Pr^{III} and Er^{III} are in between.

Using these luminescence lifetimes we can estimate the Pt→Ln energy-transfer rates k_{ET} from Equation (1), where τ_q is the residual lifetime of Pt-based emission following quenching by a lanthanide Ln, and τ_u is the "unquenched" lifetime in the reference complex with Ln = Gd (578 ns).

$$k_{ET} = \frac{1}{\tau_q} - \frac{1}{\tau_u} \quad (1)$$

This gives Pt→Ln energy-transfer rates of $>10^8\ s^{-1}$ (for Nd), $\approx 4\times10^7\ s^{-1}$ (for Pr and Er), and $2\times10^6\ s^{-1}$ (for Yb). These values may be rationalised on the basis of the spectroscopic overlap between the emission spectrum of the donor (Pt^{II} dimer) component and the absorption spectrum of the acceptor (Ln^{III}) component. Yb^{III} has just a single f–f absorption at about 980 nm (10200 cm^{-1}), which will overlap only with the very weak low-energy tail of the Pt^{II}-based emission, thereby accounting for the slow energy-transfer rate (as van Veggel et al. observed in a $[Ru(bipy)_3]^{2+}/Yb^{III}$ dyad,[7] and we observed in a $[Ru(bipy)(CN)_4]^{2-}/Yb^{III}$ coor-

dination network).[9] Although in some cases energy transfer to Yb^{III} can be faster than expected due to the possibility of an alternative redox-based mechanism for energy transfer,[14] the relative slowness of Pt→Yb energy transfer here indicates that this pathway is unlikely to be significant.

In contrast, Nd^{III} is rich in f–f excited states in the relevant region, with ten f–f levels lying between 11000 and 20000 cm^{-1} (910 and 500 nm) spanning the region where the Pt-based emission is at its most intense (see Figure 9 for the relevant lanthanide energy levels). It is easy to see, therefore, how Pt→Ln energy transfer is very much faster to Nd^{III} than to Yb^{III}. On this basis we might expect Pt→Er energy transfer to be significantly faster than Pt→Pr energy transfer. However, energy transfer to the $^4F_{9/2}$ and $^4I_{9/2}$ levels of Er^{III} is forbidden by both Förster and Dexter mechanisms. The former requires that $|\Delta J|=2$, 4 or 6 at the lanthanide, and the latter requires that $|\Delta J|=0$ or 1 (with the exception of $J=J'=0$ which is forbidden).[15] Population of the $^4F_{9/2}$ and $^4I_{9/2}$ levels of Er^{III} would require $\Delta J=3$ compared to the ground state, which is forbidden (although it is important to realise that these selection rules are not absolute but are relaxed somewhat by intensity stealing from allowed transitions such as 4f–5d).[16] Thus, Pr^{III} and Er^{III} are actually in a similar situation regarding their ability to be sensitised by energy transfer, with one low-energy f–f state at ≈10000 cm^{-1} and one higher-energy state [$^1D_2$ for Pr^{III} at ≈17500 cm^{-1}, and $^4S_{3/2}$ for Er^{III} at ≈18500 cm^{-1}; both require Förster energy transfer to be sensitised with $|\Delta J|=2$ and 6, respectively]. Higher energy f–f states are not likely to be involved; from the onset of luminescence at the high-energy end of the Pt^{II} luminescence spectrum we can estimate the energy of the ^{3}MMLCT excited state to be ≈19000 cm^{-1}, so only f–f states lower than this need to be considered. Conversely, energy levels below ≈10000 cm^{-1} are unlikely to be directly populated by energy transfer, even if it is allowed by the selection rules, because of negligible overlap with the luminescence spectra of the energy donor Pt^{II} units. In fact we know that the $^1D_2$ level of Pr^{III} has been sensitised because the 1050 nm emission peak, used to measure the Pr^{III}-based lifetime (see Figure S2, Supporting Information), has the assignment $^1D_2 \rightarrow {}^3F_4$, originating from the $^1D_2$ level.[17]

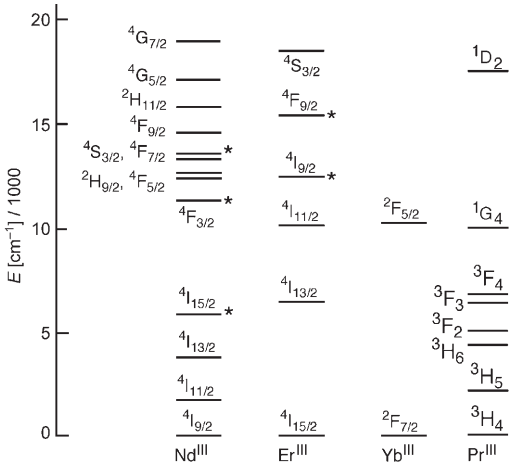

Figure 9. Low-lying energy levels of the near-IR emitting Ln^{III} cations (Ln = Yb, Nd, Er, Pr). Those labelled * are those for which population from the ground state by energy transfer is *forbidden* according to the selection rules associated with either Förster or Dexter energy transfer (see main text and ref. [15]).

Figure 10 provides an alternative way of looking at this; the bottom part of Figure 10 shows the absorption spectra of [Nd(hfac)$_3$(phen)] and [Er(hfac)$_3$(phen)], and the top part shows the Pt-based luminescence profile of [**1**·Gd(tta)$_3$]$_\infty$. It will be obvious that many of the f–f absorptions that are expected for Er^{III} and Nd^{III} on the basis of the energy-level diagram in Figure 9 actually have very low intensity and do not contribute significantly to the donor/acceptor spectroscopic overlap. The most significant f–f absorptions for Er^{III} occur in the 520–530 nm region, where the $^4S_{3/2} \leftarrow {}^4I_{15/2}$ transition is expected, split into closely-spaced components due to crystal-field effects. For Nd^{III} the most intense area of absorption is 570–600 nm, where the $^4G_{5/2} \leftarrow {}^4I_{9/2}$ transition is expected; significant lower-energy absorptions at around 750 and 800 nm may be assigned to $^4S_{3/2} \leftarrow {}^4I_{9/2}/{}^4F_{7/2} \leftarrow {}^4I_{9/2}$ transitions in the former case, and $^2H_{9/2} \leftarrow {}^4I_{9/2}/{}^4F_{5/2} \leftarrow {}^4I_{9/2}$ transitions in the latter. It will be obvious from the Figure that the ^{3}MMLCT-based emission from the Pt^{II} dimers in the [**1**·Ln(tta)$_3$]$_\infty$ series overlaps with all of these three regions of Nd^{III}-based absorption, whereas overlap with the main Er^{III}-based absorption will be small because in that region the high-energy end of the ^{3}MMLCT-based emission has barely emerged from the baseline. It is therefore easy to see why Pt$_2$(^{3}MMLCT)→Ln photoinduced energy transfer is faster to Nd^{III} than it is to Er^{III} in the [**1**·Ln(tta)$_3$]$_\infty$ series, and this is in agreement with the general pattern that we have observed in other Ru^{II}–Ln^{III} systems where the emission from the d-block component has its maximum in the 600 nm region.[9]

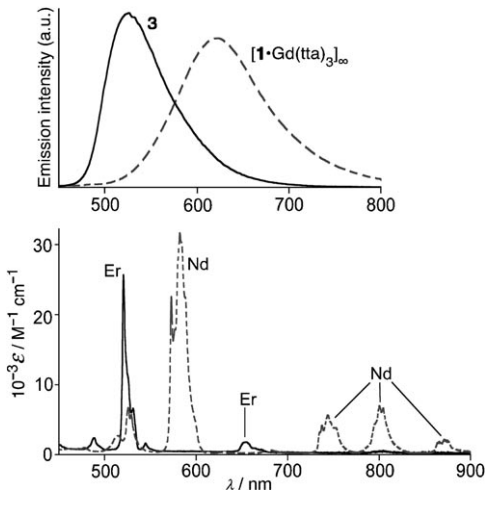

Figure 10. a) Emission profiles from **3** (^{3}MLCT based, in solution; solid line) and [**1**·Gd(tta)$_3$]$_\infty$ (^{3}MMLCT based, solid state; dashed line); and b) absorption spectra of [Ln(hfac)$_3$(phen)] in CH_2Cl_2 solution (Ln = Er, solid line; Nd, dashed line). The correspondences between the emission maximum of **3** and absorption of Er^{III}, and the emission maximum of [**1**·Gd(tta)$_3$]$_\infty$ and the absorption of Nd^{III}, are obvious.

Exactly similar behaviour was shown by the series $[\mathbf{2}\cdot Ln(hfac)_3]_\infty$ which showed ^{3}MMLCT-based emission from the Pt^{II} pairs centred at 625 nm, with the intensity decreasing in the order $[\mathbf{2}\cdot Gd(hfac)_3]_\infty > [\mathbf{2}\cdot Yb(hfac)_3]_\infty > [\mathbf{2}\cdot Er(hfac)_3]_\infty > [\mathbf{2}\cdot Nd(hfac)_3]_\infty$ according to the degree of quenching from the lanthanide centre following the arguments above. The lifetimes of the Pt-based luminescence (based on fitting the data to a single exponential function to give a value which is the weighted average of the different components, see Table 1) were 768, 413, 56 and < 10 ns, respectively, allowing estimation of the Pt→Ln energy-transfer rates k_{ET} as $> 10^8\ s^{-1}$ (for Nd), and $\approx 2\times10^7\ s^{-1}$ (for Er) and $10^6\ s^{-1}$ (for Yb), in reasonable agreement with what we observed for the series $[\mathbf{1}\cdot Ln(tta)_3]_\infty$.

Quenching of the Pt^{II}-based emission was accompanied, for all complexes containing Nd, Pr, Er or Yb, by appearance of the characteristic sensitised near-infrared luminescence from the Ln^{III} centre. The near-IR emission spectra and the lifetimes are unremarkable, being entirely representative of {Ln(diketonate)$_3$(diimine)} emitters.[8] The lifetimes are listed in Table 1 and representative emission spectra in the near-IR region are shown in the Supporting Information (Figure S2). The important point is that this lanthanide-based luminescence has arisen not by direct excitation of the lanthanide fragment, but by energy transfer from the Pt^{II}-based chromophore which was sensitised by excitation into the MLCT (or MMLCT) transition. We note that emission from Pr^{III} is particularly weak because of the ease with which it is quenched by molecular vibrations, and time-resolved measurements on Pr^{III} emission are rare.[17]

iii) Adducts of 1 and 2 with Ln^{III} diketonates in solution: Since the behaviour of the Pt^{II} fragments **1** and **2** is quite different in the coordination networks described above from that in dilute solution, due to the presence of the Pt···Pt contacts which change the nature of the emitting excited state from ^{3}MLCT to ^{3}MMLCT, we were interested also to examine the behaviour of adducts of **1** and **2** with {Ln(diketonate)$_3$} fragments in solution. We accomplished this by starting with solutions of **1** or **2** in CH_2Cl_2 and titrating in known amounts of various $[Ln(hfac)_3(H_2O)_2]$ complexes to see the effect on the absorption and emission properties of **1** and **2** when the lanthanide unit binds to the pyridyl groups pendant from the Pt^{II} complexes. The series $[Ln(hfac)_3(H_2O)_2]$ was used rather than $[Ln(tta)_3(H_2O)_2]$ because the former has no significant absorbance at wavelengths longer than 350 nm, so will not interfere with the Pt-based MLCT band in the absorption spectrum, whereas the thiophene units of $[Ln(tta)_3(H_2O)_2]$ mean that its absorption spectrum extends out to 400 nm which would hinder selective excitation of the Pt^{II} chromophores.

The effects on the absorption and emission spectra of **1** of adding aliquots of $[Gd(hfac)_3(H_2O)_2]$ to a 5 μM sample of complex **1** in CH_2Cl_2 are shown in Figure 11. At this concentration the effects of aggregation of Pt^{II} complexes can be ignored. In the absorption spectrum the MLCT band, whose maximum starts at 389 nm, approximately trebles in intensity and is blue-shifted; the band appears to be centred at about 370 nm but appears as a shoulder on the strong absorbance of the excess $[Gd(hfac)_3(H_2O)_2]$ at $\lambda < 350$ nm. This blue-shift is consistent with the Gd^{III} centre acting as an electron-withdrawing substituent on **1** when coordinated to the pendant pyridyl groups, stabilising the metal d orbitals and thereby increasing the MLCT energy gap. There is no clear isosbestic point, which is not surprising as there could be a wide range of adducts present from $(\mathbf{1})_2\cdot\{Gd(hfac)_3\}$ early in the titration to $(\mathbf{1})\cdot\{Gd(hfac)_3(H_2O)\}_2$ late in the titration, with a range of linear or cyclic adducts of intermediate stoichiometries in between. However the absorbance at 415 nm varied little during the UV/Vis titration so this wavelength was used as the excitation wavelength for the luminescence measurements.

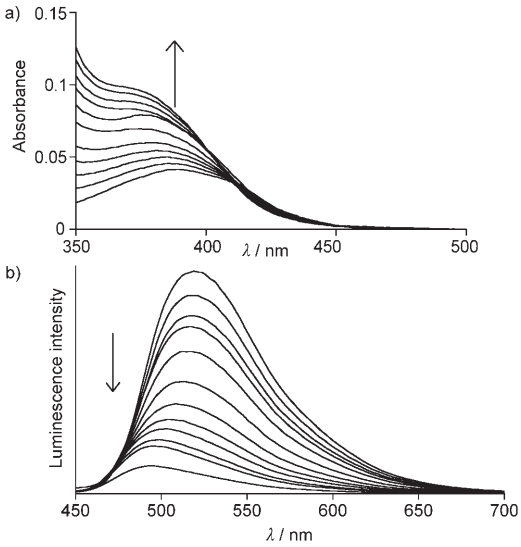

Figure 11. Changes in the a) UV/Vis absorption and b) luminescence spectra of **1** in CH_2Cl_2 solution (5 μM) associated with addition of samples of $[Nd(hfac)_3(H_2O)_2]$ (up to 4 molar equivalents).

The blue-shift of the MLCT absorption maximum of **1** as $[Gd(hfac)_3(H_2O)_2]$ is titrated in is mirrored by a blue-shift in the emission maximum, which moves from 520 up to 494 nm. However, the luminescence intensity substantially *decreases* during the titration despite the shift to higher energy. This is in apparent contravention of the energy-gap law,[18] which has been shown to apply to Pt^{II} complexes;[18c] higher-energy excited states normally display more intense luminescence because there is less likelihood of quenching by low energy molecular vibrations. Energy-transfer quenching is not possible due to the high (UV region) energy of the lowest excited state of Gd^{III}. One possible explanation is the presence of additional vibrational modes introduced by coordination of the {Gd(hfac)$_3$} units which provide additional non-radiative quenching pathways for the MLCT excited state. An alternative explanation is that raising the energy of the Pt-based ^{3}MLCT state by coordination of the electron-withdrawing {Gd(hfac)$_3$} units brings the ^{3}MLCT

state close in energy to a higher-lying short-lived, non-radiative state such as a d–d state, which provides an efficient deactivation pathway via thermally-activated equilibration between the two. This is well-known in Ru^{II}–polypyridyl chemistry, where $[Ru(bipy)_3]^{2+}$ is strongly emissive because the d–d state is sufficiently far above the ^{3}MLCT state in energy that it is not significantly populated at room temperature; but $[Ru(terpy)_2]^{2+}$ is very weakly emissive because the lower energy of the d–d state means that it can be thermally populated via the ^{3}MLCT state and then undergo fast radiationless decay.[19]

To see which of these hypotheses was correct we performed a simple control experiment, namely bubbling HCl gas through a solution of **1** in MeCN or CH_2Cl_2 and examining the spectroscopic consequences. Protonation of the pendant pyridyl groups of **1** resulted in a blue-shift of the MLCT absorption maximum to 370 nm and an approximate doubling in intensity; the luminescence was also blue-shifted to 470 nm and, significantly, substantially reduced in intensity (by $\approx$90%). These observations are exactly in agreement with the behaviour of **1** on binding of {Gd(hfac)$_3$} units. Since protonation and metallation with {Gd(hfac)$_3$} have such similar effects, it is likely that the second explanation above is the correct one, namely that raising the energy of the ^{3}MLCT level by attaching an electron-withdrawing substituent to the pyridyl groups brings it close in energy to a higher-lying non-luminescent excited state which provides a new quenching pathway. It is interesting that such an effect clearly did not occur in the solid state, when the Pt-based ^{3}MMLCT luminescence (from the Pt···Pt bonded dimer units) was very strong in the lanthanide coordination polymers; this must be because the ^{3}MMLCT state is considerably lower in energy than the ^{3}MLCT to start with.

The intensity data from the solution titrations could not be used to extract reliable stepwise formation constants for attachment of one and then two Gd^{III} fragments to the pendant pyridyl groups of **1**, because the stoichiometry of the host/guest adducts will change during the titration, as described above. However, it is clear that the lanthanide/pyridyl association is strong because the Pt-based luminescence is nearly completely quenched after addition of $\approx$10 equivalents of [Gd(hfac)$_3$(H$_2$O)$_2$] (5 μM of **1** and 50 μM of [Gd(hfac)$_3$(H$_2$O)$_2$]).

Exactly similar sequences of absorption and luminescence spectra were recorded during titrations with other [Ln(hfac)$_3$(H$_2$O)$_2$] (Ln = Nd, Er, Yb); in these cases the quenching of the Pt-based luminescence is not surprising as there is the possibility of Pt→Ln energy transfer in addition to the quenching effect described above. We could follow this by monitoring the reduction in the lifetime of the Pt-based luminophore **1** during a titration with a [Ln(hfac)$_3$(H$_2$O)$_2$] complex. Typically, as small amounts of the [Ln(hfac)$_3$(H$_2$O)$_2$] complex are titrated into a solution of **1**, the luminescence decay becomes multi-exponential with i) a relatively long component characteristic of free **1**, and ii) two shorter components which could reasonably correspond to **1** with one {Ln(hfac)$_3$(H$_2$O)} unit attached, and **1** with two {Ln(hfac)$_3$(H$_2$O)} units attached. The luminescence decays are clearly better fits to three components rather than two. A typical example is provided by titration of **1** with [Yb(hfac)$_3$(H$_2$O)$_2$] in CH_2Cl_2. At an early stage in the titration (when 0.5 equivalents of [Yb(hfac)$_3$(H$_2$O)$_2$] have been added) the three lifetime components are 137, 55 and 28 ns, with the first of these (corresponding to free **1**) being dominant. As more [Yb(hfac)$_3$(H$_2$O)$_2$] is added the longest-lived component makes a smaller contribution to the decay, as determined by the pre-exponential value, and the two shorter-lived components have a higher weighting. After addition of four equivalents of [Yb(hfac)$_3$(H$_2$O)$_2$] the long-lived component has disappeared and the dominant component of the luminescence decay is now the shortest-lived component. The intermediate-lifetime component grows in significance and then disappears again as the titration proceeds. This behaviour is shown in Figure 12 and is typical of the effects of adding any of the [Ln(hfac)$_3$(H$_2$O)$_2$] (Ln = Nd, Er, Yb) series to a solution of **1**.

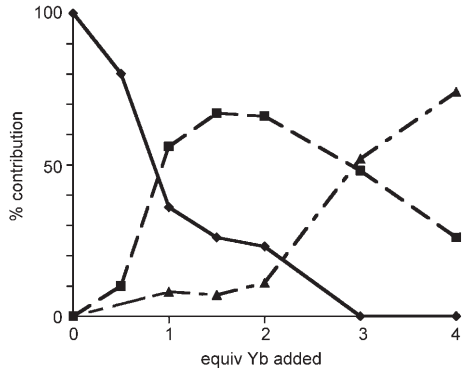

Figure 12. Relative contributions of the long, medium and short-lived luminescence components to the total emission intensity of **1** during addition of [Yb(hfac)$_3$(H$_2$O)$_2$] (up to 4 molar equivalents; see main text for further explanation).

We did not attempt to determine Pt→Ln energy-transfer rates from these solution experiments because of i) the likely presence of several adducts of different stoichiometry in solution, and ii) the fact that the Pt^{II}-based emission is essentially completely quenched in *every* case because of the effect alluded to earlier whereby a non-emissive excited state becomes thermally accessible as the ^{3}MLCT energy of the Pt^{II} unit is raised during the titration. Instead, we used complex **3** to assess energy-transfer rates in solution (next section) since this forms adducts with [Ln(hfac)$_3$(H$_2$O)$_2$] of well-defined stoichiometry.

iii) Adducts of 3 with Ln^{III} diketonates in solution: Stepwise addition of portions of [Gd(hfac)$_3$(H$_2$O)$_2$] to a solution of **3** in CH_2Cl_2 resulted in an approximate doubling of the absorption intensity throughout the broad MLCT absorption manifold (Figure 13a). The maximum has blue-shifted to 377 nm, although singling out one maximum for particular emphasis is of limited value as this broad region of absorb-

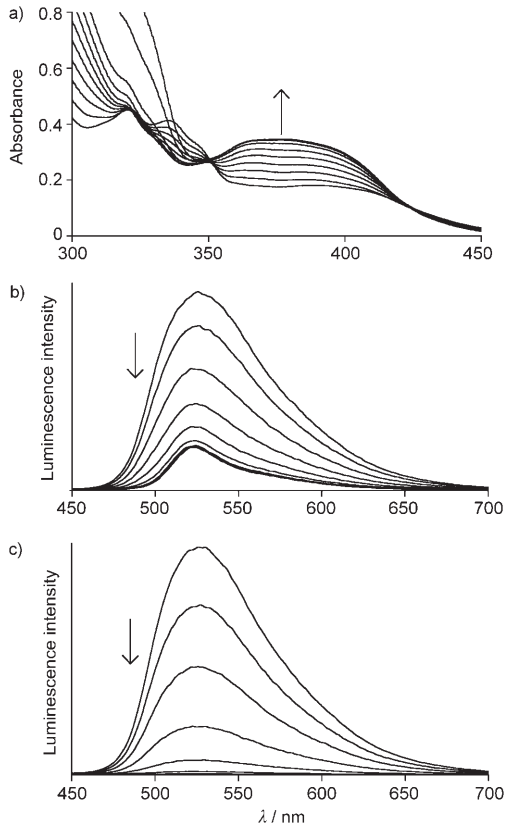

Figure 13. Changes in the a) UV/Vis absorption and b) luminescence spectra of **3** in CH_2Cl_2 solution (5 μM) associated with addition of samples of $[Gd(hfac)_3(H_2O)_2]$. c) shows an analogous titration to that in b) but using $[Nd(hfac)_3(H_2O)_2]$ instead of $[Gd(hfac)_3(H_2O)_2]$; note the now-complete quenching of Pt-based luminescence.

ance clearly contains several components. There are approximate isosbestic points at 424 and 350 nm; perfect isosbestic points are not to be expected given the presence of three different species absorbing in this region [free **3**, dinuclear **3**·{$Gd(hfac)_3$} and trinuclear **3**·{$Gd(hfac)_3\}_2$]. During this titration the luminescence intensity of **3** dimishes to 22% of its starting value, and is only slightly blue-shifted from 526 to 522 nm (Figure 13b). The small size of this blue-shift implies that in this case the {$Gd(hfac)_3$} substituents are having only a weak electron-withdrawing effect on the {Pt(bipy)} centre, possibly because of the position at which the phen group is substituted (*meta*, in contrast to *para* substitution of the pyridyl groups in complexes **1** and **2**). The reduction in luminescence intensity can be ascribed to the same effect that we saw with **1** and **2**, that is, the involvement of a non-luminescent higher-lying excited state which becomes thermally accessible, although the effect is clearly much weaker here allowing the residual luminescence of the Pt^{II} centre of **3** in the presence of {$Gd(hfac)_3$} substituents to be seen clearly. From a plot of Δ(absorbance) versus amount of added $[Gd(hfac)_3(H_2O)_2]$ it is clear that the association is strong, with a straight-line change until two equivalents of $[Gd(hfac)_3(H_2O)_2]$ are added and no further change thereafter. Given the concentrations of $\approx 10^{-5}$ M used for these experiments it is clear that the two stepwise association constants are each $\gg 10^5\,M^{-1}$, which is reasonable; unsubstituted phenanthroline binds to lanthanide tris(diketonates) to form [Ln(diketonate)$_3$(phen)] adducts with association constants of about $10^7\,M^{-1}$ in low-polarity solvents.[20] In trinuclear **3**·{$Gd(hfac)_3\}_2$ in CH_2Cl_2 solution the lifetime of the Pt-centred MLCT luminescence increases by more than a factor of 2, to 835 ns. This is consistent with an electron-withdrawing effect arising from the {$Gd(hfac)_3$} substituents, which was just apparent from the blue-shift in the emission wavelength, resulting in a higher-energy ^{3}MLCT state and hence increased lifetime due to the energy-gap law.

Clearly different behaviour occurs when Ln^{III} ions other than Gd^{III} are used, that is, on titration of **3** with aliquots of $[Ln(hfac)_3(H_2O)_2]$ (Ln = Yb, Nd, Er). In these cases the luminescence is nearly completely quenched (Figure 13c), and the residual Pt-based MLCT emission has a much *shorter* lifetime (17 ns for Ln = Yb, 7 ns for Ln = Nd and ≈1 ns for Ln = Er). This is now consistent with energy transfer occurring from the Pt-based ^{3}MLCT state to the Ln^{III} centre, with rate constants of $6\times10^7\,s^{-1}$ for Pt→Yb energy transfer, $1.4\times10^8\,s^{-1}$ for Pt→Nd energy transfer and $>10^9\,s^{-1}$ for Pt→Er energy transfer. As we saw in the solid-state coordination networks based on **1** and **2**, the energy transfer is slowest to Yb^{III} because it has only a single f–f accepting level at a low energy (10200 cm^{-1}) which will provide very poor overlap with the donor emission spectrum. However, in contrast to what we observed earlier, Pt→Er energy transfer is now faster than Pt→Nd energy transfer, with Er^{III} being the more effective quencher of the Pt^{II}-based emission. This may be explained with reference to Figure 10. The Pt^{II}-based ^{3}MLCT luminescence maximum of **3** (526 nm in solution) is at higher energy than the ^{3}MMLCT luminescence from [**1**·$Ln(tta)_3]_\infty$ or [**2**·$Ln(hfac)_3]_\infty$ (630 nm in the solid state), and now overlaps well with the principal f–f absorption manifold of Er^{III}. Conversely the overlap of luminescence from **3** with the Nd^{III}-based f–f absorptions is poorer as the main Nd^{III}-based absorptions only overlap with the low-energy tail of luminescence from **3**. Thus the high-energy ^{3}MLCT luminescence of **3** overlaps better with the Er^{III}-based f–f absorptions, whereas the lower-energy ^{3}MMLCT-based luminescence of [**1**·$Ln(tta)_3]_\infty$ or [**2**·$Ln(hfac)_3]_\infty$ overlaps better with the Nd^{III}-based f–f absorptions, explaining the relative Pt→Ln energy-transfer rates in these systems.

It is noticeable that all three energy-transfer rates for the adducts **3**·{$Ln(hfac)_3\}_2$ are much faster than was observed for the corresponding lanthanides in the series of solid-state materials [**1**·$Ln(tta)_3]_\infty$ and [**2**·$Ln(hfac)_3]_\infty$, although given the quite different characteristics of the energy donor in each case {^{3}MLCT in [**3**·{$Ln(hfac)_3\}_2$], versus ^{3}MMLCT in [**1**·$Ln(tta)_3]_\infty$ and [**2**·$Ln(hfac)_3]_\infty$}, and the different electronic pathways connecting the Pt and Ln metal centres, direct comparison is not appropriate. Part of the effect must however reflect the slightly shorter Pt···Ln separation in the series [**3**·{$Ln(hfac)_3\}_2$] (8.4 Å for the adducts of **3** compared with 9.9 Å for the adducts of **1** and **2**). This is a small difference but given the high distance dependence[21] of both För-

ster energy transfer (r^{-6}) and Dexter energy transfer (e^{-r}) this will amount to an increase in energy-transfer rates of factors of 2.7 or 4.5 according to the Förster or Dexter mechanisms, respectively, even before any other factors are taken into account.

As we expected, and have observed in other cases,[8,9] the quenching of the Pt-based ^{3}MLCT luminescence in the adducts [**3**•{Ln(hfac)$_3$}$_2$] (Ln = Yb, Nd, Pr, Er) was accompanied by the appearance of sensitised Ln-based luminescence in the near-IR region following Pt→Ln energy transfer. The lifetimes of these are typical for {Ln(diketonate)$_3$(diimine)} chromophores (≈11, 2, 1 and 0.1 μs for Yb, Er, Nd and Pr, respectively; see Table 1) and need no further discussion. The important point is again that this sensitised emission was observed from the Ln^{III} centres following selective excitation into the tail of the Pt-based MLCT absorption at 440 nm, a wavelength where the {Ln(diketonate)$_3$(diimine)} units do not themselves absorb, and must therefore have arisen from Pt→Ln energy transfer. For solid [**3**•{Ln(hfac)$_3$}$_2$] (Ln = Yb, Nd) essentially identical results were obtained, with excitation of the Pt chromophore at 440 nm affording Yb or Nd-based emission with lifetimes of ≈11 and 1 μs respectively.

Conclusion

The complexes **1**–**3** contain Pt(bipy)(diacetylide) chromophores with pendant pyridyl or phenanthroline groups to which {Ln(diketonate)$_3$} fragments can coordinate; for **1** and **2** this results in formation of one-dimensional coordination polymers [**1**•Ln(tta)$_3$]$_\infty$ and [**2**•Ln(hfac)$_3$]$_\infty$, whereas **3** forms simpler trinuclear adducts [**3**•{Ln(hfac)$_3$}$_2$]. In solution complexes **1**–**3** show Pt^{II}-centred ^{3}MLCT luminescence between 508 and 526 nm, which is quenched by addition of {Ln(diketonate)$_3$} fragments. For **3** this quenching is associated (for Ln = Yb, Nd, Er which have low-energy f–f excited states) with Pt→Ln energy transfer resulting in sensitised near-infrared luminescence characteristic of these Ln^{III} ions. For **1** in solution, however, the quenching arises from a shift of the Pt^{II}-based ^{3}MLCT transition to higher energy following coordination of the {Ln(diketonate)$_3$} fragment; we believe that this increase in the ^{3}MLCT energy brings it energetically close to a higher-lying non-radiative excited state which provides an efficient quenching pathway. In the solid state in contrast, [**1**•Ln(tta)$_3$]$_\infty$ and [**1**•Ln(hfac)$_3$]$_\infty$ contain pairs of Pt(bipy)(diacetylide) chromophores which are associated by a short Pt···Pt interaction such that the chromophore now has ^{3}MMLCT character rather than ^{3}MLCT character, and luminescence at lower energies (ca. 630 nm) than the monomeric Pt^{II} complexes. In the adducts containing Yb, Nd^{III}, Er^{III} or Pr^{III} the Pt^{II}-based ^{3}MMLCT luminescence is quenched to an extent depending on the ability of the different Ln^{III} ions to act as energy acceptors, with Yb^{III} providing the least quenching (slowest Pt→Ln energy transfer) and either Nd^{III} or Er^{III} providing the most (fastest Pt→Ln energy transfer) depending on whether the Pt^{II}-based emission comes from an ^{3}MLCT state [better overlap with the absorption spectrum of Er^{III}] or a lower-energy ^{3}MMLCT state [better overlap with the absorption spectrum of Nd^{III}]. As a whole this series of complexes provides structurally interesting examples of materials in which near-infrared Ln^{III}-based luminescence can be sensitised using either ^{3}MLCT or ^{3}MMLCT excited-states of Pt(bipy)(diacetylide) chromophores.

Experimental Section

General details: [Pt(dmso)$_2$Cl$_2$],[22] 4-ethynylpyridine,[23] Ln(diketonate)$_3$•2H$_2$O[24] (diketonate = tta, hfac) and 3-ethynyl-1,10-phenanthroline[25] were prepared according to literature methods. All other reagents were obtained from commercial sources (Avocado, Aldrich) and used as received. Dry solvents were purchased from Aldrich or obtained from a Grubbs dry solvent system.

UV/Vis spectra were measured on a Cary-50 instrument; IR spectra were measured as KBr pellets on a Perkin-Elmer Spectrum One instrument. Steady-state luminescence spectra were measured on a Perkin–Elmer LS50B fluorimeter, using a front surface accessory in the case of powder samples. ^{1}H NMR spectra were recorded on a Bruker AC-250 or Bruker AMX2-400 spectrometer, and all mass spectra on a VG AutoSpec magnetic sector instrument.

Luminescence lifetimes in the visible region, of both solution and powder samples, were measured using an Edinburgh Instruments Mini-τ instrument fitted with a 405 nm pulsed diode laser as excitation source and a cooled Hamamatsu-R928 PMT detector; wavelength selection at the detector was by means of 50 nm bandpass filters. Typically a minimum of 10000 counts was accumulated for the decay curve, from which lifetimes were extracted using the supplied software from Edinburgh Instruments. Lifetimes of lanthanide-based luminescence in the near-IR region were measured using an experimental setup that has been described previously.[26] Steady-state emission spectra in the near-IR region were measured using a Jobin-Yvon Spex Fluorolog-3 spectrometer with a Xe lamp as excitation source and a Hamamatsu R5509–73 photomultiplier tube as detector.

Preparation of PtLCl$_2$ (L=bipy, 4,4′-*t*Bu$_2$-bipy): A mixture of [Pt(dmso)$_2$Cl$_2$] (0.21 g, 0.5 mmol) and the appropriate ligand L (1 equiv) in degassed acetonitrile (30 mL) was heated to reflux under N$_2$ for 24 h. The reaction mixture was then cooled to 0 °C and the resulting yellow precipitate was filtered off, washed with hexane and ether, and dried. All characterization data matched those previously reported.[27]

Preparation of 1: A mixture of [Pt(bipy)Cl$_2$] (0.49 g, 1.2 mmol), anhydrous CuI (50 mg, catalyst), and dry *i*Pr$_2$NH (14 mL) in dry, degassed dichloromethane (60 mL) under N$_2$ was stirred for 10 min, after which 4-ethynylpyridine (0.36 g, 3.5 mmol, 3 equiv) was added. The resulting suspension was stirred under N$_2$ at room temperature protected from light for 5 d. The solvent was evaporated and the solid residue was dried in vacuo to remove traces of *i*Pr$_2$NH. The product was purified by column chromatography on alumina, eluting with CH$_2$Cl$_2$/MeOH 97:3. Yield: 0.48 g, 75%; ^{1}H NMR (400 MHz, CDCl$_3$): δ = 9.71 (dd, 2H; bipy H^6), 8.45 (m, 4H; py H^2), 8.19 (td, 2H; bipy H^4), 8.11 (d, 2H; bipy H^3), 7.76 (td, 2H; bipy H^5), 7.66 ppm (m, 4H; py H^3); ^{13}C NMR (100 MHz, CDCl$_3$): δ = 156.1, 151.7, 149.1, 139.1, 135.8, 127.8, 126.5, 122.4, 100.4, 92.8 ppm; IR (KBr disk): $\tilde{\nu}$ = 3112 (w), 3045 (w), 3024 (w), 2925 (w), 2853 (w), 2131 (s), 2119 (s), 1608 (w), 1592 (s), 1530 (m), 1485 (m), 1472 (w), 1449 (m), 1431 (w), 1415 (w), 1404 (w), 1316 (w), 1248 (w), 1211 (m), 1160 (m), 1062 (w), 1037 (w), 989 (m), 822 (s), 759 (s), 723 (m), 566 (m), 549 cm^{-1} (m); FAB MS: *m*/*z*: 556 [*M*+H]$^+$; elemental analysis calcd (%) for PtC$_{24}$H$_{16}$N$_4$: C 51.9, H 2.9, N 10.1; found: C 51.9, H 2.9, N 10.0; X-ray quality crystals were grown by slow evaporation of a CH$_2$Cl$_2$ solution.

Preparation of 2: A mixture of [Pt(4,4′-*t*Bu$_2$bipy)Cl$_2$] (0.72 g, 1.4 mmol), anhydrous CuI (50 mg, catalyst), and dry *i*Pr$_2$NH (13 mL) in dry, degassed dichloromethane (150 mL) under N_2 was stirred for 10 min, after which 4-ethynylpyridine (0.33 g, 3.2 mmol, 2 equiv) was added. The resulting suspension was stirred under N_2 at room temperature protected from light for 5 d. The solvent was evaporated and the solid residue was dried in vacuo to remove traces of *i*Pr$_2$NH. The product was purified by column chromatography on alumina, eluting with CH_2Cl_2/MeOH 99:1. Yield: 0.74 g, 82%; ^{1}H NMR (400 MHz, $CDCl_3$): $\delta = 9.53$ (d, 2H; bipy H^6), 8.44 (d, 4H; py H^2), 7.97 (d, 2H; bipy H^3), 7.61 (dd, 2H; bipy H^5), 7.34 (m, 4H; py H^3), 1.44 ppm (s, 18H; C(CH$_3$)$_3$); ^{13}C NMR (100 MHz, $CDCl_3$): $\delta = 164.1$, 156.1, 151.1, 148.8, 136.3, 126.6, 124.9, 118.9, 100.1, 94.5, 35.9, 30.2 ppm; IR (KBr disk): $\tilde{\nu}$ = 3066 (w), 3015 (w), 2964 (m), 2906 (w), 2870 (w), 2126 (s), 2112 (s), 1618 (m), 1588 (s), 1545 (w), 1531 (w), 1484 (m), 1462 (w), 1417 (m), 1366 (w), 1251 (w), 1208 (m), 1120 (w), 1032 (w), 989 (m), 901 (w), 874 (w), 841 (w), 821 (s), 740 (w), 600 (m), 570 (m), 543 cm^{-1} (m); FAB MS: *m*/*z*: 668 [*M*+H]$^+$; elemental analysis calcd (%) for $PtC_{32}H_{32}N_4{\cdot}0.5\,CH_2Cl_2$: C 55.0, H 4.7, N 7.9; found: C 55.3, H 4.7, N 7.7; X-ray quality crystals were grown by slow evaporation of a CH_2Cl_2 solution.

Preparation of 3: A mixture of [Pt(4,4′-*t*Bu$_2$bipy)Cl$_2$] (0.110 g, 0.18 mmol), dry *i*Pr$_2$NH (2 mL) and anhydrous CuI (9 mg) in dry, degassed dichloromethane (30 mL) was stirred at room temperature under dry N_2 for 10 min, after which 3-ethynyl-1,10-phenanthroline (0.089 g, 0.44 mmol) was added. The resulting suspension was stirred under N_2 at room temperature protected from light for 5 d. The solvent was evaporated and the solid residue was dried in vacuo to remove traces of *i*Pr$_2$NH. The product was purified by column chromatography on alumina, eluting with CH_2Cl_2/MeOH 95:5. Yield: 0.047 g, 30%; ^{1}H NMR (500 MHz, [D$_6$]DMSO): $\delta = 9.55$ (d, 2H; bipy H^6), 9.10 (d, 2H; phen H^2), 9.07 (dd, 2H; phen H^9), 8.73 (d, 2H; bipy H^3), 8.45 (m, 4H; phen H^{4,7}), 7.97 (m, 6H; bipy H^5 and phen H^{5,6}), 7.72 (dd, 2H; phen H^8), 1.45 ppm (s, 18H; C(CH$_3$)$_3$); FAB MS: *m*/*z*: 870 [*M*+H]$^+$; elemental analysis calcd (%) for $C_{46}H_{38}N_6Pt{\cdot}0.5\,CH_2Cl_2$: C 61.2, H 4.3, N 9.2; found: C 60.9, H 4.1, N 9.4.

Preparation of coordination polymers [1·Ln(tta)$_3$]$_\infty$: A solution of **1** ($\approx$0.05 mmol) in CH_2Cl_2 was slowly mixed with a solution of the appropriate [Ln(tta)$_3$]·2H$_2$O (1 equiv) in CH_2Cl_2 by putting the component solutions into the separate arms of an H-tube and allowing the solutions to mix slowly by diffusion. The polymers formed as orange microcrystalline solids which were filtered off and washed with hexane.

Data for [1·Yb(tta)$_3$]$_\infty$: Yield: 47%; IR (KBr disk): $\tilde{\nu}$=3112 (w), 3080 (w), 2129 (s), 2119 (s), 1607 (s), 1541 (s), 1505 (m), 1450 (m), 1413 (s), 1353 (m), 1307 (s), 1248 (m), 1231 (m), 1211 (m), 1183 (s), 1143 (s), 1085 (w), 1062 (m), 1007 (m), 936 (w), 859 (w), 833 (m), 785 (s), 768 (w), 758 (m), 724 (m), 682 (w), 643 (m), 582 (m), 545 cm^{-1} (w); elemental analysis calcd (%) for $PtYbC_{48}H_{28}N_4F_9O_6S_3{\cdot}0.5\,CH_2Cl_2$: C 40.6, H 2.0, N 3.9; found: C 40.5, H 1.8, N 3.9.

Data for [1·Er(tta)$_3$]$_\infty$: Yield: 60%; IR (KBr disk): $\tilde{\nu}$=3113 (w), 3080 (w), 2128 (s), 2118 (s), 1606 (s), 1540 (s), 1505 (m), 1450 (m), 1413 (s), 1353 (m), 1306 (s), 1248 (m), 1231 (m), 1211 (m), 1186 (s), 1143 (s), 1085 (w), 1062 (m), 1007 (m), 935 (w), 859 (w), 833 (m), 785 (s), 768 (w), 758 (m), 723 (m), 681 (w), 643 (m), 582 (m), 545 cm^{-1} (w); elemental analysis calcd (%) for $PtErC_{48}H_{28}N_4F_9O_6S_3$: C 41.6, H 2.0, N 4.0; found: C 41.3, H 1.9, N 4.0.

Data for [1·Gd(tta)$_3$]$_\infty$: Yield: 42%; IR (KBr disk): $\tilde{\nu}$=3113 (w), 3081 (w), 2129 (s), 2118 (s), 1605 (s), 1539 (s), 1504 (m), 1450 (m), 1413 (s), 1355 (m), 1303 (s), 1248 (m), 1231 (m), 1211 (m), 1186 (s), 1143 (s), 1085 (w), 1062 (m), 1007 (m), 934 (w), 859 (w), 832 (m), 786 (s), 768 (w), 758 (m), 724 (m), 681 (w), 642 (m), 581 (m), 545 cm^{-1} (w); elemental analysis calcd (%) for $PtGdC_{48}H_{28}N_4F_9O_6S_3.CH_2Cl_2$: C 40.3, H 2.1, N 3.8; found: C 40.6, H 2.1, N 3.8.

Data for [1·Pr(tta)$_3$]$_\infty$: Yield: 48%; IR (KBr disk): $\tilde{\nu}$=3114 (w), 3081 (w), 2131 (s), 2120 (s), 1603 (s), 1537 (s), 1504 (m), 1450 (m), 1412 (s), 1354 (m), 1299 (s), 1248 (m), 1230 (m), 1211 (m), 1183 (s), 1143 (s), 1085 (w), 1062 (m), 1006 (m), 933 (w), 859 (w), 832 (m), 786 (s), 767 (w), 758 (m), 723 (m), 681 (w), 641 (m), 580 (m), 544 cm^{-1} (w); elemental analysis calcd (%) for $PtPrC_{48}H_{28}N_4F_9O_6S_3{\cdot}0.5\,CH_2Cl_2$: C 41.5, H 2.1, N 4.0; found: C 41.7, H 2.0, N 4.0.

Data for [1·Nd(tta)$_3$]$_\infty$: Yield: 52%; IR (KBr disk): $\tilde{\nu}$=3113 (w), 3080 (w), 2131 (s), 2120 (s), 1603 (s), 1538 (s), 1503 (m), 1450 (m), 1413 (s), 1354 (m), 1299 (s), 1248 (m), 1230 (m), 1211 (m), 1183 (s), 1143 (s), 1085 (w), 1062 (m), 1006 (m), 933 (w), 859 (w), 832 (m), 786 (s), 767 (w), 758 (m), 723 (m), 681 (w), 641 (m), 580 (m), 544 cm^{-1} (w); elemental analysis calcd (%) for $PtNdC_{48}H_{28}N_4F_9O_6S_3$: C 42.3, H 2.1, N 4.1; found: C 41.9, H 1.9, N 4.0.

Preparation of coordination polymers [2·Ln(hfac)$_3$]$_\infty$: A solution of **2** ($\approx$0.05 mmol) in CH_2Cl_2 was added to a solution of the appropriate Ln(hfac)$_3$·2H$_2$O (1 equiv) in CH_2Cl_2 and the mixture was stirred overnight. The polymers precipitated over a few hours as orange microcrystalline solids overnight which were filtered off and washed with hexane. If the mixture was not stirred but was just left to stand overnight, X-ray quality crystals were formed.

Data for [2·Yb(hfac)$_3$]$_\infty$: Yield: 46%; IR (KBr disk): $\tilde{\nu}$=3145 (w), 3086 (w), 2972 (w), 2877 (w), 2128 (m), 2120 (m), 1655 (s), 1608 (s), 1558 (m), 1532 (m), 1489 (m), 1469 (m), 1427 (w), 1419 (w), 1255 (s), 1213 (s), 1146 (s), 1105 (m), 1009 (m), 844 (w), 833 (m), 800 (m), 741 (w), 661 (m), 600 (w), 587 cm^{-1} (m); elemental analysis calcd (%) for $PtYbC_{47}H_{35}N_4F_{18}O_6$: C 38.6, H 2.4, N 3.8; found: C 38.2, H 2.1, N 3.5.

Data for [2·Er(hfac)$_3$]$_\infty$: Yield: 64%; IR (KBr disk): $\tilde{\nu}$=3145 (w), 3086 (w), 2972 (w), 2876 (w), 2128 (m), 2119 (m), 1655 (s), 1608 (s), 1558 (m), 1532 (m), 1489 (m), 1468 (m), 1427 (w), 1419 (w), 1255 (s), 1213 (s), 1146 (s), 1104 (m), 1010 (m), 844 (w), 833 (m), 800 (m), 741 (w), 661 (m), 600 (w), 586 cm^{-1} (m); elemental analysis calcd (%) for $PtErC_{47}H_{35}N_4F_{18}O_6{\cdot}2\,CH_2Cl_2$: C 36.2, H 2.4, N 3.5; found: C 36.3, H 2.4, N 3.9.

Data for [2·Gd(hfac)$_3$]$_\infty$: Yield: 77%; IR (KBr disk): $\tilde{\nu}$=3145 (w), 3086 (w), 2972 (w), 2876 (w), 2127 (m), 2117 (m), 1653 (s), 1607 (s), 1557 (m), 1531 (m), 1489 (m), 1468 (m), 1427 (w), 1419 (w), 1255 (s), 1213 (s), 1145 (s), 1101 (m), 1009 (m), 844 (w), 832 (m), 800 (m), 741 (w), 660 (m), 601 (w), 585 cm^{-1} (m), elemental analysis calcd (%) for $PtGdC_{47}H_{35}N_4F_{18}O_6{\cdot}0.5\,CH_2Cl_2$: C 38.3, H 2.4, N 3.8; found: C 38.4, H 2.3, N 3.8.

Data for [2·Nd(hfac)$_3$]$_\infty$: Yield: 53%; IR (KBr disk): $\tilde{\nu}$=3145 (w), 3083 (w), 2972 (w), 2877 (w), 2127 (m), 2118 (m), 1652 (s), 1606 (s), 1556 (m), 1530 (m), 1487 (m), 1468 (s), 1419 (w), 1254 (s), 1213 (s), 1146 (s), 1099 (m), 1007 (m), 843 (w), 832 (m), 800 (m), 740 (w), 660 (m), 601 (w), 584 cm^{-1} (m); elemental analysis calcd (%) for $PtNdC_{47}H_{35}N_4F_{18}O_6$ requires: C 39.4, H 2.5, N 3.9; found: C 39.0, H 2.2, N 3.9.

Preparation of trinuclear complexes [3·{Ln(hfac)$_3$}$_2$]: A mixture of complex **3** (43 mg, 0.05 mmol) and 2 equiv of the appropriate Ln(hfac)$_3$·(H$_2$O)$_2$ (Ln = Nd, Yb) were placed in a sample vial and a small amount of heptane was added. Dichloromethane was added dropwise to the above mixture until the solids were dissolved. The system was left to evaporate slowly until solid precipitates of the desired compounds were appeared (ca. 2 d). The solids were filtered, washed with hexane and dried. For Ln = Yb X-ray quality crystals were obtained.

Data for [3·{Nd(hfac)$_3$}$_2$]: Yield 68%; elemental analysis calcd (%) for $PtNd_2C_{76}H_{44}N_6F_{36}O_{12}$: C 38.0, H 1.9, N 3.5; found: C 37.6, H 1.8, N 3.4.

Data for [3·{Yb(hfac)$_3$}$_2$]: Yield 72%; elemental analysis calcd (%) for $PtYb_2C_{76}H_{44}N_6F_{36}O_{12}$: C 37.1, H 1.8, N 3.4; found: C 37.4, H 1.9, N 3.1.

Photophysical studies on other members of this series were performed by preparing the complexes in situ from **3** plus two equivalents of the appropriate Ln(hfac)$_3$·(H$_2$O)$_2$ without isolation of the solid adducts.

X-ray crystallography: Data for crystals of **1** and [**3**·{Yb(hfac)$_3$}$_2$·(CH_2Cl_2)$_{1.5}$] were collected at the University of Sheffield using a Bruker SMART-1000 diffractometer equipped with graphite-monochromatized $Mo_{K\alpha}$ radiation. Data for crystals of [**1**·Yb(tta)$_3$·(CH_2Cl_2)$_{1.5}$]$_\infty$ and [**1**·Er(tta)$_3$·(CH_2Cl_2)$_{1.5}$]$_\infty$ were collected at the National Crystallography Service, University of Southampton, on a Nonius KappaCCD diffractometer using $Mo_{K\alpha}$ radiation (λ = 0.71073 Å) from a Bruker-Nonius FR591 rotating anode X-ray generator. Data for crystals of **2**·(CH_2Cl_2)$_{0.5}$, [**2**·Er(hfac)$_3$·(CH_2Cl_2)]$_\infty$ and [**2**·Yb(hfac)$_3$·(CH_2Cl_2)]$_\infty$ were collected at the Daresbury Synchrotron Radiation Source (station 9.8) using a Bruker SMART-APEX2 diffractometer and Si(111)-monochromatized synchrotron radiation with a wavelength close to the Zr absorption edge. In all

Table 2. Crystallographic data for the seven new structures.

Compound	**1**	**2**$(CH_2Cl_2)_{0.5}$	[**1**·Yb(tta)$_3$·$(CH_2Cl_2)_{1.5}]_\infty$	[**1**·Er(tta)$_3$·$(CH_2Cl_2)_{1.5}]_\infty$	[**2**·Yb(hfac)$_3$·$(CH_2Cl_2)]_\infty$	[**2**·Er(hfac)$_3$·$(CH_2Cl_2)]_\infty$	[**3**·{Yb(hfac)$_3$}$_2$·$(CH_2Cl_2)_{1.5}$]
empirical formula	$C_{24}H_{16}N_4Pt$	$C_{32.5}H_{33}ClN_4Pt$	$C_{49.5}H_{32}Cl_3F_9N_4O_4PtS_3Yb$	$C_{49.5}H_{32}Cl_3ErF_9N_4O_4PtS_3$	$C_{48}H_{37}Cl_2F_{18}N_4O_6PtYb$	$C_{48}H_{37}Cl_2ErF_{18}N_4O_6Pt$	$C_{77.5}H_{46}Cl_3F_{36}N_6O_{12}PtYb_2$
F_w	555.50	710.17	1520.45	1514.67	1546.85	1541.07	2584.72
diffractometer	Bruker	Bruker	Bruker	Bruker	Bruker	Bruker	Bruker
	SMART-1000	SMART-APEX2	Nonius KappaCCD	Nonius KappaCCD	SMART-APEX2	SMART-APEX2	SMART-1000
λ [Å]	0.71073	0.6751	0.71073	0.71073	0.6709	0.6709	0.71073
T [K]	123(2)	120(2)	120(2)	120(2)	120(2)	120(2)	150(2)
crystal size [mm]	$0.20\times0.12\times0.05$	$0.15\times0.12\times0.08$	$0.16\times0.02\times0.01$	$0.12\times0.02\times0.01$	$0.15\times0.05\times0.05$	$0.18\times0.04\times0.02$	$0.44\times0.19\times0.12$
system, space group	monoclinic, $P2_1/c$	monoclinic, $C2/c$	monoclinic, $C2/c$	monoclinic, $C2/c$	triclinic, $P\bar{1}$	triclinic, $P\bar{1}$	triclinic, $P\bar{1}$
a [Å]	13.4014(14)	21.827(3)	27.276(6)	27.197(5)	16.108(6)	16.111(6)	14.513(3)
b [Å]	6.7056(6)	15.950(2)	27.506(6)	27.682(6)	19.108(6)	19.115(7)	16.997(4)
c [Å]	21.9459(16)	18.498(3)	15.343(3)	15.316(3)	19.224(8)	19.232(6)	20.894(4)
α [°]	90	90	90	90	70.461(8)	70.296(7)	76.590(4)
β [°]	91.437(6)	104.978(2)	104.55(3)	104.23(3)	81.691(5)	81.422(4)	72.288(5)
γ [°]	90	90	90	90	77.937(6)	77.781(4)	67.466(4)
V [Å^3]	1971.5(3)	6221.1(15)	11142(4)	11177(4)	5435(3)	5430(3)	4496.0(16)
Z	4	8	8	8	4	4	2
data, restraints, parameters	3449, 0, 262	9344, 2, 352	12761, 7, 703	12744, 7, 703	37320, 73, 1444	36428, 55, 1444	20074, 716, 1231
μ [mm^{-1}]	7.134	4.623	4.513	4.327	4.492	4.319	3.840
$R1$ $[I>2\sigma(I)]$, w$R2$[a]	0.0371, 0.0944	0.0400, 0.1252	0.0358, 0.0906	0.0645, 0.1274	0.0892, 0.2846	0.0547, 0.1476	0.0686, 0.1907

[a] $R1=\Sigma||F_o|-|F_c||/\Sigma|F_o|$ for "observed data"; w$R2=[\Sigma w(F_o^2-F_c^2)^2/\Sigma w(F_o^2)^2]^{1/2}$ for all unique data.

cases, the data were absorption corrected using SADABS[28] before solution and refinement using SHELXS-97 and SHELXL-97, respectively.[29] Details of the crystal data and data collection and refinement parameters are summarised in Table 2.

The refinements of the structures of **1** and **2**·$(CH_2Cl_2)_{0.5}$ were straightforward and presented no problems; in the latter case the CH_2Cl_2 molecule was in a general position but refined most sensibly with a site occupancy of 50%. In the structures of [**1**·Yb(tta)$_3$·$(CH_2Cl_2)_{1.5}]_\infty$ and [**1**·Yb(tta)$_3$·$(CH_2Cl_2)_{1.5}]_\infty$, one CH_2Cl_2 molecule has its C atom disordered over two positions and this atom was refined with isotropic displacement parameters; the other CH_2Cl_2 molecule refined most sensibly with a site occupancy of 50%.

Both [**2**·Er(hfac)$_3$·$(CH_2Cl_2)]_\infty$ and [**2**·Yb(hfac)$_3$·$(CH_2Cl_2)]_\infty$ contain two formula units [that is, two independent Pt^{II} and two independent Ln^{III} centres, and two independent CH_2Cl_2 molecules] in the asymmetric unit; in one of the CH_2Cl_2 molecules the two Cl atoms are each disordered over two sites. In addition two of the CF_3 groups [based on C(109) and C(115) for the Er^{III} complex and C(110) and C(120) for the Yb^{III} complex] show rotational disorder such that their F atoms were disordered over two sites each; these six partial F atoms were refined isotropically. In both cases the crystals were twinned; for [**2**·Yb(hfac)$_3$·$(CH_2Cl_2)]_\infty$, whose crystals showed the weaker scattering of the two, this resulted in difficulties in applying an accurate absorption correction, resulting in large residual electron-density peaks close to the metal atoms and a relatively poor refinement ($R1=0.089$). However the structural discussion in the main text is based on the isostructural compound [**2**·Er(hfac)$_3$·$(CH_2Cl_2)]_\infty$ for which better data were obtained and which gave a reasonable refinement of $R1=0.055$.

In [**3**·{Yb(hfac)$_3$}$_2$·$(CH_2Cl_2)_{1.5}$], one CH_2Cl_2 molecule is in a general position and the other is disordered across an inversion centre with 50% in the asymmetric unit. Half of the CF_3 groups [those based on atoms C(37), C(42), C(47) C(71), C(72), C(76)] exhibit rotational disorder such that the attached F atoms are disordered over two sites; these F atoms were refined isotropically, with extensive use of restraints to keep the C–F and non-bonded F···F distances reasonable.

A few significant bond lengths are included in the relevant Figure captions; for full tables of bond lengths and angles, see Supporting Information.

CCDC-608093–608099 contain the supplementary crystallographic data for this paper. These data can be obtained free of charge from the Cambridge Crystallographic Data Centre via www.ccdc.cam.ac.uk/data_request/cif.

Acknowledgements

We thank the New Zealand Tertiary Education Commission for a Top Achiever Doctoral scholarship to T.K.R., EPSRC (UK) for grants to T.L. and S.J.A.P. and for funding of the UK National Crystallography Service, and CCLRC (UK) for access to synchrotron facilities.

[1] a) S. Faulkner, J. L. Matthews, "Fluorescent complexes for biomedical applications" in *Comprehensive Coordination Chemistry*, *Vol. 9* (Ed.: M. D. Ward,), Elsevier, Oxford, **2004**, 2nd ed., pp. 913; b) G. R. Motson, J. S. Fleming, S. Brooker, *Adv. Inorg. Chem.* **2004**, *55*, 361; c) J.-C. G. Bünzli, C. Piguet, *Chem. Soc. Rev.* **2005**, *34*, 1048.

[2] a) F. X. Zang, Z. R. Hong, W. L. Li, M. T. Li, X. Y. Sun, *Appl. Phys. Lett.* **2004**, *84*, 2679; b) H. Suzuki, *J. Photochem. Photobiol. A* **2004**, *166*, 155; c) S. Tanabe, *Comptes Rendus Chimie* **2002**, **5**, 815.

[3] N. Sabbatini, M. Guardigli, J.-M. Lehn, *Coord. Chem. Rev.* **1993**, *123*, 201.

[4] a) A. P. Bassett, R. van Deun, P. Nockemann, P. B. Glover, B. M. Kariuki, K. van Hecke, L. van Meervelt, Z. Pikramenou, *Inorg. Chem.* **2005**, *44*, 6140; b) G. Mancino, A. J. Ferguson, A. Beeby, N. J. Long, T. S. Jones, *J. Am. Chem. Soc.* **2005**, *127*, 524.

[5] S. Torelli, D. Imbert, M. Cantuel, G. Bernardinelli, S. Delahaye, A. Jauser, J.-C. G. Bünzli, C. Piguet, *Chem. Eur. J.* **2005**, *11*, 3228.

[6] Representative recent examples: a) B. P. Burton-Pye, S. L. Heath, S. Faulkner, *Dalton Trans.* **2005**, 146; b) J. Hamblin, N. Abboyi, M. P. Lowe, *Chem. Commun.* **2005**, 657; c) G. M. Davies, H. Adams, S. J. A. Pope, S. Faulkner, M. D. Ward, *Photochem. Photobiol. Sci.* **2005**, *4*, 829; d) J. Zhang, P. D. Badger, S. J. Geib, S. Petoud, *Angew. Chem.* **2005**, *117*, 2564; *Angew. Chem. Int. Ed.* **2005**, *44*, 2508; e) R. van Deun, P. Nockemann, P. Fias, K. van Hecke, L. van Meervelt, K. Binnemans, *Chem. Commun.* **2005**, 590; f) S. Kaizaki, D. Shirotani, Y. Tsukahara H. Nakata, *Eur. J. Inorg. Chem.* **2005**, 3503; g) D. Imbert, S. Comby, A.-S. Chauvin, J.-C. G. Bünzli, *Chem. Commun.* **2005**, 1432; h) S. Quici, M. Cavazzini, G. Marzanni, G. Accorsi, N. Armaroli, B. Ventura, F. Barigelletti, *Inorg. Chem.* **2005**, *44*, 529; i) G. A. Hebbink, L. Grave, L. A. Woldering, D. N. Reinhoudt, F. C. J. M. van Veggel, *J. Phys. Chem. A* **2003**, *107*, 2483.

[7] a) S. I. Klink, H. Keizer, F. C. J. M. van Veggel, *Angew. Chem.* **2000**, *112*, 4489; *Angew. Chem. Int. Ed.* **2000**, *39*, 4319; b) A. Beeby, R. S. Dickins, S. FitzGerald, L. J. Govenlock, C. L. Maupin, D. Parker, J. P. Riehl, G. Siligardi, J. A. G. Williams, *Chem. Commun.* **2000**, 1183; c) W.-K. Wong, A. Hou, J. Guo, H. He, L. Zhang, W.-Y. Wong, K.-F. Li, K.-W. Cheah, F. Xue, T. C. W. Mak, *J. Chem. Soc. Dalton Trans.* **2001**, 3092; d) D. Imbert, M. Cantuel, J.-C. G. Bünzli, G. Bernardinelli and Piguet, *J. Am. Chem. Soc.* **2003**, *125*, 15698; e) S. J. A. Pope, B. J. Coe, S. Faulkner, *Chem. Commun.* **2004**, 1550; f) S. J. A. Pope, B. J. Coe, S. Faulkner, E. V. Bichenkova, X. Yu, K. T. Douglas, *J. Am. Chem. Soc.* **2004**, *126*, 9490; g) D. Guo, C. Duan, F. Lu, Y. Hasegawa, Q. Meng, S. Yanagida, *Chem. Commun.* **2004**, 1486; h) P. B. Glover, P. R. Ashton, L. J. Childs, A. Rodger, M. Kercher, R. M. Williams, L. De Cola, Z. Pikramenou, *J. Am. Chem. Soc.* **2003**, *125*, 9918; i) S. J. A. Pope, B. J. Coe, S. Faulkner, R. H. Laye, *Dalton Trans.* **2005**, 1482; j) H.-B. Xu, L.-X. Shi, E. Ma, L.-Y. Zhang, Q.-H. Wei, Z.-N. Chen, *Chem. Commun.* **2006**, 1601.

[8] a) N. M. Shavaleev, L. P. Moorcraft, S. J. A. Pope, Z. R. Bell, S. Faulkner, M. D. Ward, *Chem. Commun.* **2003**, 1134; b) N. M. Shavaleev, L, P. Moorcraft, S, J. A. Pope, Z, R. Bell, S. Faulkner, M. D. Ward, *Chem. Eur. J.* **2003**, *9*, 5283; c) N. M. Shavaleev, Z. R. Bell, G. Accorsi, M. D. Ward, *Inorg. Chim. Acta* **2003**, *351*, 159; d) N. M. Shavaleev, G. Accorsi, D. Virgili, Z. R. Bell, T. Lazarides, G. Calogero, N. Armaroli, M. D. Ward, *Inorg. Chem.* **2005**, *44*, 61.

[9] a) T. A. Miller, J. C. Jeffery, M. D. Ward, H. Adams, S. J. A. Pope, S. Faulkner, *J. Chem. Soc. Dalton Trans.* **2004**, 1524; b) G. M. Davies, S. J. A. Pope, H. Adams, S. Faulkner, M. D. Ward, *Inorg. Chem.* **2005**, *44*, 4656; c) J.-M. Herrera, S. J. A. Pope, H. Adams, S. Faulkner, M. D. Ward, *Inorg. Chem.* **2006**, *45*, 3895.

[10] a) S. L. James, M. Younus, P. R. Raithby, J. Lewis, *J. Organomet. Chem.* **1997**, *542*, 233; b) M. Hissler, M. Connick, D. K. Geiger, J. E. McGarrah, D. Lipa, R. J. Lachiotte, R. Eisenberg, *Inorg. Chem.* **2000**, *39*, 447; c) E. C. Whittle, J. A. Weinstein, M. W. George, K. S. Schanze, *Inorg. Chem.* **2001**, *40*, 4053; d) S.-C. Chan, M. C. W. Chan, Y. Wang, C.-M. Che, K.-K. Cheung, N. Zhu, *Chem. Eur. J.* **2001**, *7*, 4180; e) F. Hua, S. Kinayyigit, J. R. Cable, F. N. Castellano, *Inorg. Chem.* **2005**, *44*, 471; f) E. O. Danilov, I. E. Pomestchenko, S. Kinayyigit, P. L. Gentili, M. Hissler, R. Ziessel, F. N. Castellano, *J. Phys. Chem. A* **2005**, *109*, 2465; g) L. Zhang, Y.-H. Niu, A. K.-Y Jen, W. Lin, *Chem. Commun.* **2005**, 1002.

[11] N. M. Shavaleev, Z. R. Bell, T. L. Easun, R. Rutkaite, L. Swanson, M. D. Ward, *Dalton Trans.* **2004**, 3678.

[12] W. Lu, M. C. W. Chan, N. Zhu, C.-M. Che, Z. He, K.-Y. Wong, *Chem. Eur. J.* **2003**, *9*, 6155.

[13] a) V. H. Houlding, V. M. Miskowski, *Coord. Chem. Rev.* **1991**, *111*, 145; b) M. Kato, C. Kosuge, K. Morii, J. S. Ahn, H. Kitagawa, T. Mitani, M. Matsushita, T. Kato, S. Yano, M. Kimura, *Inorg. Chem.* **1999**, *38*, 1638; c) W. B, Connick, L. M. Henling, R. E. Marsh, H. B. Gray, *Inorg. Chem.* **1996**, *35*, 6261; d) G. Arena, G. Calogero, S. Campagna, L. M. Scolaro, V. Ricevuto, R. Romeo, *Inorg. Chem.* **1998**, *37*, 2763; e) U. Siemeling, K. Bausch, H. Fink, C. Bruhn, M. Baldus, B. Angerstein, R. Plessow, A Brockhinke, *Dalton Trans.* **2005**, 2365; f) H.-F. Xiang, S.-C. Chan, K. K.-Y. Wu, C.-M. Che, P. T. Lai, *Chem. Commun.* **2005**, 1408; g) M. Hissler, J. E. McGarrah, W. B. Connick, D. K. Geiger, S. D. Cummings, R. Eisenberg, *Coord. Chem. Rev.* **2000**, *208*, 115; h) V. W.-W. Yam, K. M.-C. Wong, N. Zhu, *J. Am. Chem. Soc.* **2002**, *124*, 6506.

[14] a) S. Faulkner, B. P. Burton-Pye, T. Khan, L. R. Martin, S. D. Wray, P. J. Skabara, *Chem. Commun.* **2002**, 1668; b) A. Beeby, S. Faulkner, J. A. G. Williams, *J. Chem. Soc. Dalton Trans.* **2002**, 1918; c) W. D. Horrocks, Jr., J. P. Bolender, W. D. Smith, R. M. Supkowski, *J. Am. Chem. Soc.* **1997**, *119*, 5972.

[15] G. F. de Sá, O. L. Malta, C. de Mello Donegá, A. M. Simas, R. L. Longo, P. A. Santa-Cruz, E. F. da Silva Jr., *Coord. Chem. Rev.* **2000**, *196*, 165.

[16] G. Blasse, B. C. Grabmaier, *Luminescent materials*, Springer, Berlin, **1994**.

[17] a) A. I. Voloshin, N. M. Shavaleev, V. P. Kazakov, *J. Lumin.* **2001**, *93*, 199; b) E. B. Sveshnikova, N. T. Timofeev, *Opt. Spektrosk.* **1980**, *48*, 503; c) G. M. Davies, H. Adams, S. J. A. Pope, S. Faulkner, M. D. Ward, *Photochem. Photobiol. Sci.* **2005**, *4*, 829; d) G. M. Davies, R. J. Aarons, G. R. Motson, J. C. Jeffery, H. Adams, S. Faulkner, M. D. Ward, *Dalton Trans.* **2004**, 1136.

[18] a) R. Engelman, J. Jortner, *Mol. Phys.* **1970**, *18*, 145; b) W. Siebrand, *J. Chem. Phys.* **1967**, *47*, 2411; c) S. D. Cummings, R. Eisenberg, *J. Am. Chem. Soc.* **1996**, *118*, 1949.

[19] A. Juris, V. Balzani, F. Barigelletti, S. Campagna, P. Belser, A. Von Zelewsky, *Coord. Chem. Rev.* **1988**, *84*, 85.

[20] a) K. Iftikhar, M. Sayeed, N. Ahmad, *Inorg. Chem.* **1982**, *21*, 80; b) S. Yajima, Y. Hasegawa, *Bull. Chem. Soc. Japan* **1998**, *71*, 2825.

[21] a) D. L. Dexter, *J. Chem. Phys.* **1953**, *21*, 836; b) T. Förster, *Discuss. Faraday Soc.* **1957**, *27*, 7; c) J. R. Lakowicz, *Principles of fluorescence spectroscopy*, Kluwer Academic/Plenum Publishers, New York, 2nd ed., **1999**.

[22] J. H. Price, A. N. Williamson, R. F. Schramm, B. B. Wayland, *Inorg. Chem.* **1972**, *11*, 1280.

[23] L. D. Ciana, A. Haim, *J. Heterocycl. Chem.* **1984**, *21*, 607.

[24] Y. Hasegawa, Y. Kimura, K. Murakoshi, Y. Wada, J. Kim, N. Nakashima, T. Yamanaka, S. Yanagida, *J. Phys. Chem.* **1996**, *100*, 10201.

[25] a) C. Michel, D. Habibi, M. Schmittel, *Molecules* **2001**, *6*, M224; b) C. Michel, D. Habibi, M. Schmittel, *Molecules* **2001**, *6*, M225.

[26] N. M. Shavaleev, S. J. A. Pope, Z. R. Bell, S. Faulkner, M. D. Ward, *Dalton Trans.* **2003**, 808.

[27] G. T. Morgan and F. H. Burstall, *J. Chem. Soc.* **1934**, 965.

[28] G. M. Sheldrick, SADABS version 2.10; University of Göttingen, **2003**.

[29] G. M. Sheldrick, SHELXS-97 and SHELXL-97; University of Göttingen, **1997**.

Received: May 18, 2006
Published online: September 22, 2006

